

Chapter 22

Multi-Photon 3D Lithography and Calcination for sub-100-nm Additive Manufacturing of Inorganics



Greta Merkininkaitė, Edvinas Aleksandravičius, Simonas Varapnickas, Darius Gailevičius, Simas Šakirzanovas, and Mangirdas Malinauskas

Abstract Development of 3D micro-/nanostructures leads to device miniaturization, enhanced function, and advanced integration opportunities in the fields of photonics, micro-fluidics, micro-mechanics, micro-electronics, and micro-optics. Multi-photon lithography (also widely known as two-photon polymerization) as a laser direct writing technique offers the flexibility to rapidly prototype 3D structure for additive manufacturing. Recent developments of this ultrafast laser technique together with the advances in material science allowed routine 3D printing of inorganic structures via a combination of mask-less photopolymerization and thermal post-treatment (pyrolysis and/or calcination). The present achievements are very promising for technical applications where highly resilient structures (made out of inert and durable materials) are required to withstand harsh environments, for high-intensity optics applications in open space industry.

In this chapter, the physical and chemical principles for 3D nanostructuring of inorganics are covered via laser lithography of hybrid and composite materials with subsequent post-treatment. The most recent advances are overviewed, and the major achievements are highlighted including resilient sub-100-nm feature fabrication made of crystalline nanostructures, with a high refractive index and transparency.

G. Merkininkaitė

Faculty of Chemistry and Geoscience, Vilnius University, Vilnius, Lithuania

Femtika, Vilnius, Lithuania

e-mail: greta.merkininkaite@chgf.vu.lt

E. Aleksandravičius · S. Varapnickas · D. Gailevičius · M. Malinauskas (✉)

Laser Research Center, Physics Faculty, Vilnius University, Vilnius, Lithuania

e-mail: edvinas.aleksandravicius@ff.vu.lt; simonas.varapnickas@ff.vu.lt;

darius.gailevicius@ff.vu.lt; mangirdas.malinauskas@ff.vu.lt

S. Šakirzanovas

Faculty of Chemistry and Geoscience, Vilnius University, Vilnius, Lithuania

Department of Chemical Engineering and Technology, Center for Physical Sciences and Technology, Vilnius, Lithuania

e-mail: simas.sakirzanovas@chf.vu.lt

Advances and limitations within the context of the emerging trends and potential near-future applications are discussed in detail.

Keywords Ultrafast laser · 3D nanostructuring · Two-photon polymerization · Non-linear lithography · Post-processing · hybrid polymers; SZ2080TM · Inorganics

Abbreviations

3D	Three dimensional
λ	Wavelength
τ	Pulse duration
f	Frequency
P_{avg}	Average measured laser beam power
v	Scan velocity
AAAPs	α -amino-alkylaceto-phenones
AESO	Acrylated epoxidized soy oil
D	Donor
DFW	Dynamic fabrication window
DH	Donor hydrogen
DIW	Extrusion-based direct ink writing
DLP	Digital light processing
fs	Femtosecond
FW	Fabrication window
HAPs	Hydroxy-aceto-phenones
IJP	Inkjet-based inkjet printing
LDW	Laser direct write
M	Monomer
MEMS	Microelectromechanical systems
MMMP	Methyl-1-(4-methylthio)phenyl-2-morpholinopropan-1-one
MPL	Multi-photon lithography
NEMS	Nanoelectromechanical systems
PI	Photoinitiator
R	Radical
SL	Stereolithography
STED	Stimulated emission depletion
TPP	Two-photon polymerization

1 Introduction

Multi-photon 3D lithography [1] (specifically, two-photon polymerization TPP [2]) is already a well-established technique among scientists and readily available in the industry [3]. Its versatility meets the requirements for a plethora of micro- and nano-scale applications where true 3D structures and high-feature definition are needed [4]. It can be extended to larger dimensions of up to mm-scales (upscaled) with a wide variety of materials to choose from [5, 6].

By definition, the outcomes of the photopolymerization processes are inherently related to the spectrum of cross-linkable materials. The materials can be purely organic or at least have some organic constituents [7]. This is indeed acceptable to a great extent for prototyping and additive manufacturing of micro-optics, nanophotonics, micro-fluidics, micro-mechanics, biomedicine, sensor, and diverse templating (master or mask-making) applications [8]. However, organic or enhanced hybrid organic–inorganic resins have limited their laser direct write (LDW) empowered advantages for manufacturing complex architectures and especially integrated devices. Such devices must feature high performance and durability under harsh conditions.

On the other hand, glasses, ceramics, and crystals offer unique properties as technical materials for high resilience, transparency, and low-inertia materials. Thus, technology for making inorganic structures has been developed to meet these needs. The first example is sol–gel (solid–gel) chemistry and its combination with high-temperature post-processing. The former relates to pyrolysis (from the Greek-derived element *pyro*—fire and *lysis*—separating) and calcination (derives its name from the Latin *calcinare*—meaning to burn lime). Pyrolysis starts from $>400\text{ }^{\circ}\text{C}$ with an inertial atmosphere (vacuum, nitrogen, argon) as organic molecules are chemically altered and then evaporate. In contrast, calcination typically requires a higher temperature and an air (oxidative) atmosphere to change the material to a completely inorganic substance. In addition, these are not the only observable effects. For sol–gel resists, designed for multi-photon polymerization, heat treatment with increasing temperature causes an increase in the cross-linking degree (hard bake), partial material removal, and densification together with geometrical downscaling. Furthermore, at elevated temperatures $>1000\text{ }^{\circ}\text{C}$) inorganic glass–ceramic material phases can be observed followed by the emergence of crystalline phases. This, besides being a very interesting study object on its own, together with the inevitable shrinkage, can produce unique advantages (or disadvantages). It may depend on the application; however, this offers simultaneous geometry and material tuning to produce devices unachievable using different methods.

Up to now, the 3D printing of sol–gel materials and manufacturing of inorganic structures were limited to the micro-scale. However, recent advances in femtosecond laser material processing enabled research achieving features on the nano-scale. With a combination of ultrafast lasers (both, short pulses and high repetition rates), the 3D lithography is becoming a precision additive manufacturing tool with $\sim 100\text{-nm}$ spatial definition (resolution) on demand (see for instance Chap. 12

by S. Juodkasis). And combined with pyrolysis/calcination post-treatment enables reaching extreme scales of sub-100 nm and fabrication of true inorganic features. This is a milestone achievement in ultrafast laser nanostructuring, and in the following sections will be discussed in detail in respect of physical–chemical principles, technological realization, examples of novel emerging applications, and a future outlook.

1.1 Physical Principles of Nano-Localized Photopolymerization

A non-linear thresholded photoresponse of polymeric material is exploited for the laser direct write (LDW) 3D nanopolymerization [6, 8] as shown in Fig. 22.1. The photo-excitation of the organic monomer (prepolymer) molecules can be utilized as a linear, non-linear, super-linear light–matter interaction via single-photon, two-photon, three-photon absorption mechanisms. Additionally, during exposure, avalanche ionization and thermal accumulation might occur. The interplay between these processes is not trivial. To illustrate this, one could consider the process of two-photon polymerization. In theory, if the photon energy is at least half of the energy bandgap, two-photon absorption could be responsible for the irreversible modification converting monomers to polymers through radical polymerization (or adequate cross-linking reactions). In practice, it rarely occurs exclusively and competes with single- or three-photon absorption (depending on the applied exposure wavelength) and avalanche ionization (depends mostly on pulse duration) as well as thermal accumulation (depends a lot on pulse repetition rate). This topic is still under debate, as diverse light sources, polymer materials, and photo-initiating systems, or even exposure strategies have been exploited. Although the technique is being widely used and commercially established, still intensive research effort is being invested to better understand the fundamental processes. This is illustrated in some recent prominent review papers on that topic [6, 9]. Furthermore, a decade-long dispute about the dominant mechanisms is still in progress via original research dedicated papers [10, 11].

Nevertheless, most often a local localized photo-chemical modification (Fig. 22.2) can be achieved by optimizing light exposure parameters. Usually, this includes intensity I [W/cm^2] and corresponding energy dose D [J] for the specific material to fit within the fabrication window (FW, or a dynamic DFW taking into account the ratio of damage and initiation thresholds). Fine-tuning these values can ensure fine 3D structuring (Fig. 22.4). The final feature dimensions and resulting resolution will depend on the interplay between laser exposure (I , D), material response (sensitivity, diffusion), and geometrical rigidity (architecture)—thus in turn will be defined by physical, chemical, and engineering thresholds [6]. The routinely observed spatial dimensions of single voxels are down to 100-nm lateral and 300-nm longitudinal dimensions. And the production throughput can reach tens of thousands of individual voxels per second, which makes it an extremely efficient precision additive manufacturing tool [5, 12].

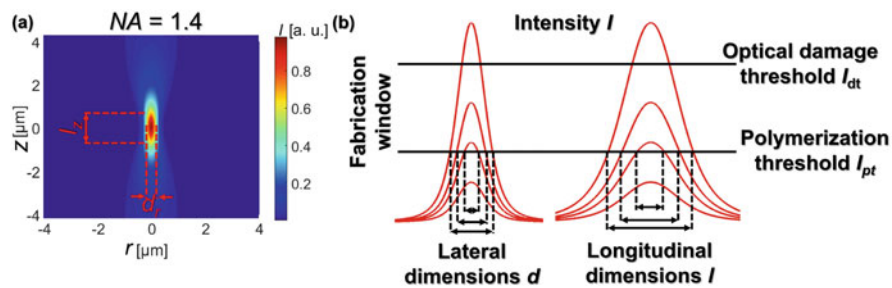


Fig. 22.1 Non-linear thresholded photoresponse of a photopolymer (prepolymer) material confined by the incident light's intensity spatial distribution. **(a)** Light intensity distribution using $NA = 1.4$ immersion oil objective. The photomodified volume is defined by the lateral d_r and axial l_z isointensity region exceeding the non-linear absorption threshold (corresponding to the highest photon density). The *voxel* (volumetric pixel) is elongated along beam propagation direction following the incident energy density distribution. r and z depict realistic probable dimensions in spatial units, while I is normalized. **(b)** Scaling by intensity tuning: lateral and longitudinal dimensions d and l fitting within the polymerization threshold (irreversible photomodification) and damage threshold (bubbling, explosions, uncontrolled burning), one can linearly vary the cross-linked volume from sub-wavelength to wavelength dimensions (lateral). The axial dimensions will be enlarged depending on the focusing optics and will follow quadratic dependence on NA . Figure adapted from [6], courtesy of Mr. E. Skliutas

1.2 Chemical Principles of Thresholded Photopolymerization

The photopolymerization process from a chemical perspective is based on the interaction between light radiations with photoinitiator and monomer. The mechanism of free radical polymerization is shown in Fig. 22.2. Free radical polymerization consists of four fundamental steps: initiation, propagation, chain transfer, and termination.

Initiation involves the formation of radicals followed by the absorbance of photons. Initiators must have an intense tendency to split into two fragments with unpaired electrons after absorption of the required energy photon. The most commonly used initiating molecules are photochemically degradable aldehydes or ketones [14]. In general, cleavage occurs at any weak bond but usually takes place at the α -position of the carbonyl group and less frequently at the β -cleavage Fig. 22.2b. The main effective chemical families of such type photoinitiators are: hydroxy-aceto-phenones, benzylketals, benzoin derivatives, α -amino-alkylaceto-phenones, phosphine oxides, α -haloaceto-phenones, trichloro-methyl-S-triazine, and others [13]. Chemical formulas of all structures (photoinitiators and monomers) are shown in Sect. 2 (Table 22.1). Basically, following radicals generation, active species then react with any monomer having an activated double bond such as α , β -unsaturated aldehydes/ketones, acrylates, vinyl esters, vinyl sulfones, imidazoles, maleimides, etc. During this process, a photoinitiator free radical adds one of the electrons to the double bond of monomer, and the remaining electron becomes the new free radical ($R_{(1)} - M$)*. In this way, chain initiation consists of two described steps (Fig. 22.2a), initiation part).

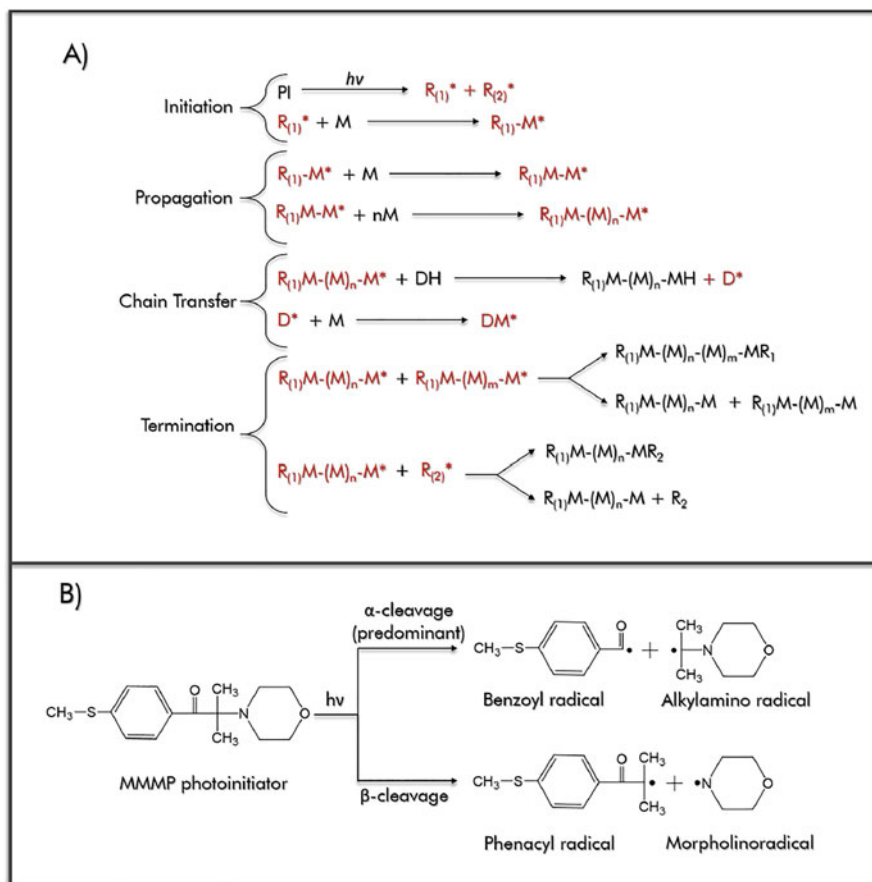
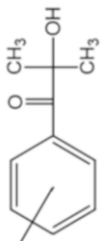
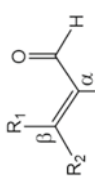
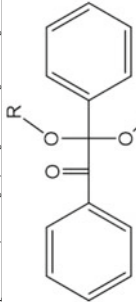
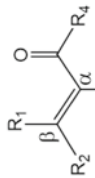
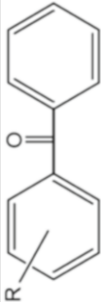
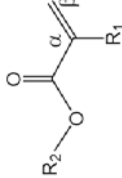


Fig. 22.2 (a) Steps of the free radical polymerization including initiation, propagation, chain transfer, and termination. PI, photoinitiator; M, monomer; D, donor; R, radical. Red markings show the active ingredient that is either causing the reaction or the result of it. (b) Photocleavage example of methyl-1-(4-methylthio)phenyl-2-morpholinopropan-1-one (MMMP) photoinitiator. Figure reproduced from [13]

During propagation, a polymer increases its chain length by the fast and progressive addition of monomers to the growing polymer chain keeping active centers. Ideally, the propagation step would continue until all monomers are consumed. However, pairs of radicals also tend to react with each other, annihilating their activities. Such behavior is called termination and is schematically depicted in Fig. 22.2a termination part.

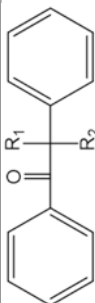
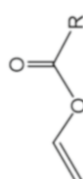
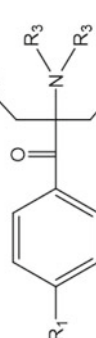
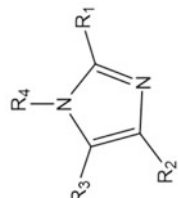
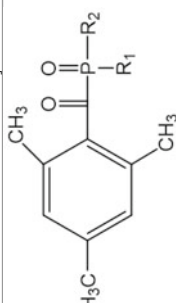
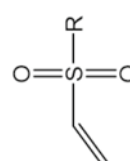
Short polymer chains can be formed due to side reaction called chain transfer. This reaction can be caused by a small molecule, such as chain transfer agent, solvent, initiator, monomer or polymer, which in the scheme corresponds to DH (Fig. 22.2a, chain transfer). Chain transfer effect results in the destruction of one

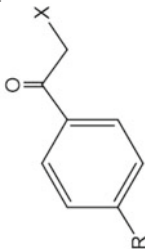
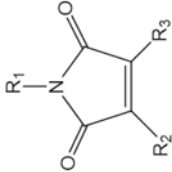
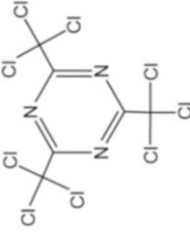
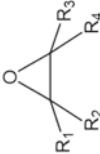
Table 22.1 Possible photoinitiators and monomers families for UV lithography

Nr.	PI group name	PI structure	Monomer name	Monomer structure
1.	Hydroxy-aceto-phenones (HAPs)	 [R: H, alkyl, hydroxyalkyloxy]	α , β -unsaturated aldehydes	
2.	Benzylketals	 [R: alkyl]	α , β -unsaturated ketones	
3.	Benzo-phenone	 [R: H, phenyl, tolythio]	α , β -unsaturated acrylates	

(continued)

Table 22.1 (continued)

Nr.	PI group name	PI structure	Monomer name	Monomer structure
4.	Benzoin derivatives	 <p>[R₁: H, OH, CH₃, alkoxy, -O-CH₂CH₂-O-, R₂: H, CH₃, O-CH₃, C₂H₅]</p>	Vinyl esters	
5.	α -amino-alkylaceto-phenones (AAAPs)	 <p>[R₁: H, -CH₃O, CH₃S, (CH₃)₂N, R₂: H, C₆H₅, CH₂=CH, R₃: CH₃, -C₂H₄OC₂H₄-]</p>	Imidazoles	
6.	Phosphine oxides	 <p>[R₁: alkyl, alkyloxy, benzyl, R₂: phenyl, ethoxy]</p>	Vinyl sulfones	

7.	<p>α-haloaceto-phenone</p>  <p>[R: alkyl, aryl, ether, (hetero)cycloalkyl, OH, X: Cl, Br]</p>	Maleimides	
8.	<p>Trichloro-methyl-S-triazine</p> 	Epoxides	

radical, but also the creation of another radical in contrast to the other modes of termination. In many cases, however, a newly created radical is unable to propagate further [15].

1.3 Laser 3D Lithography as Nano-Scale Additive Manufacturing

Combining ultrafast laser excitation with localized photopolymerization chemistry together, it can be successfully employed for LDW 3D nanolithography, in other words—optical 3D nanoprinting of cross-linkable materials. To achieve this on a basic level, a system comprising a pulsed-laser source, beam delivery/focusing, and scanning means must be used, see Fig. 22.3. Such systems are fully compatible with hybrid polymers, especially sol–gel synthesized, which can be optimized for perfect LDW 3D production due to their easy sample handling and exposure trajectory while being in a gel state, chemical wet development and superior mechanical properties to survive the whole process till revealing intricate 3D object. Finally,

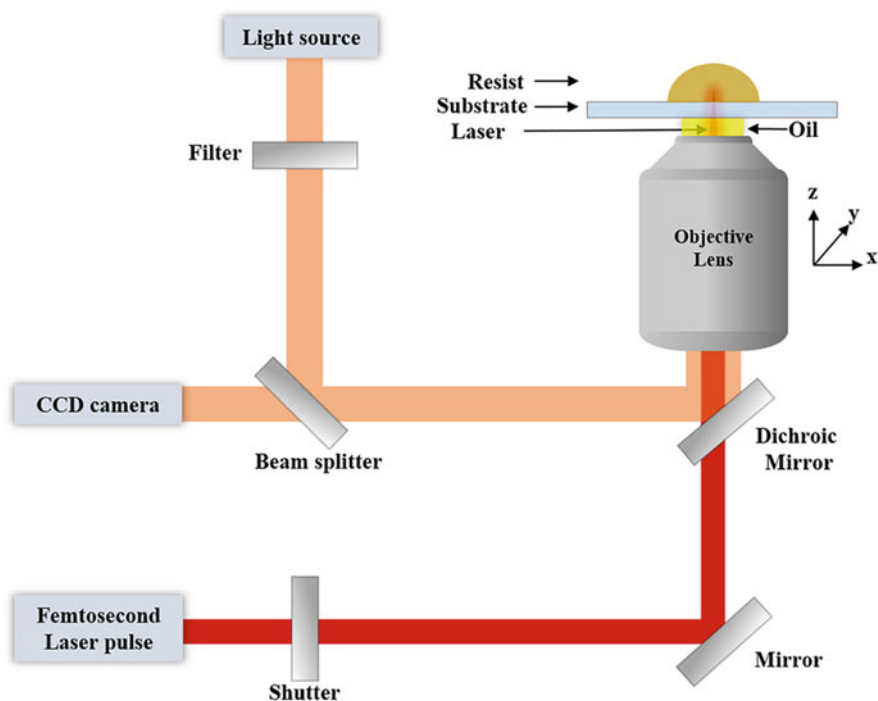


Fig. 22.3 Simplified schematic of a direct laser lithography (DLL) system operating in MPL high-resolution mode employing immersion oil objective lens. Taken from [16]

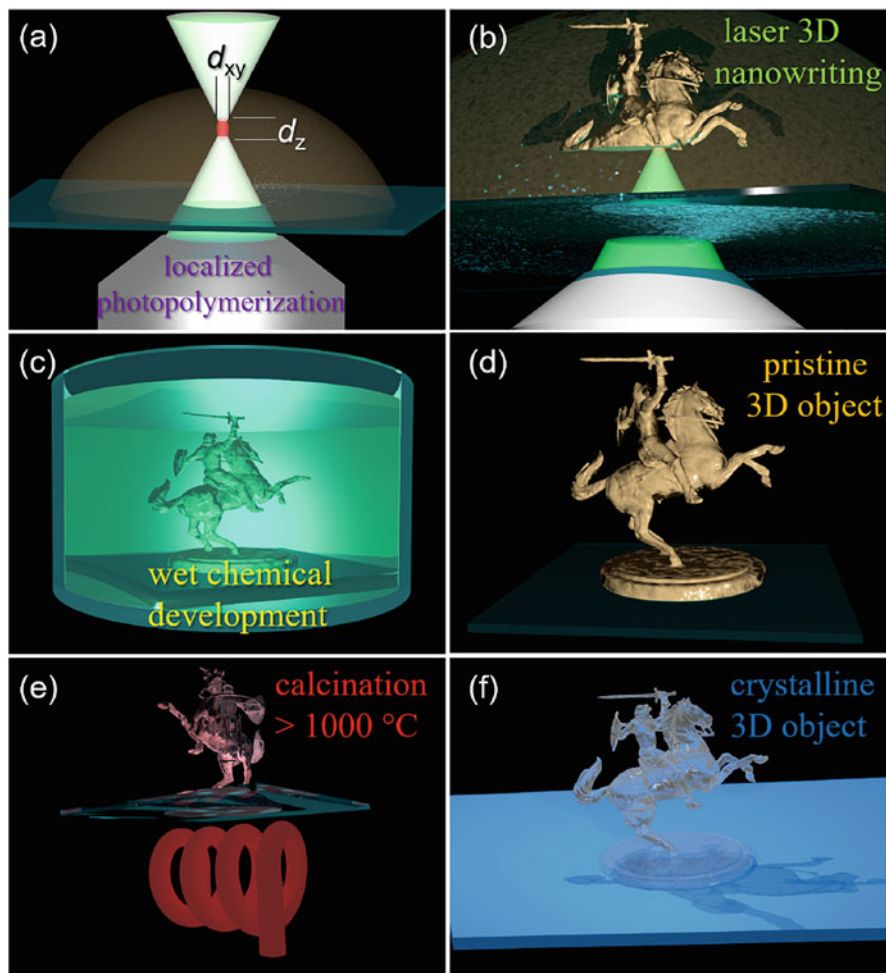


Fig. 22.4 Illustration of LDW process and heat treatment. (a) shows the basic building block of the structure—the “voxel” characterized by its transverse and longitudinal dimensions, (b) is the process of sequentially scanning the prepolymer and forming the desired structure, (c) is the development process to remove the unexposed material, (d) 3D polymeric structure, (e) calcination via thermal post-processing as a route for ceramic 3D nanostructures production, (f) shows crystalline 3D structure

the produced structures can serve as templates for various post-processing solutions including plasma etching, metal sputtering, atomic layer deposition, replications, infiltration as well as a sequence of them. For the context of this chapter’s scope, it is important that heat treatment for enhanced cross-linking [17], down-scaling [18], chemical decomposition [19], and phase change is possible [20]. The typical sequenced protocol scheme is shown in Fig. 22.4. Altogether, it can be

readily exploited for LDW as a method for additive manufacturing of inorganic substances at a nano-scale dimension. In contrast, only subtractive nanolithography was available up to now (as described in Chap. 20 by A. Rodenas).

2 Materials and Methods

Hybrid metal-organic prepolymers are outstanding materials for 3D laser printing applications. These compounds have excellent properties for fabrication, such as photosensitivity to radiation, transparency, and homogeneity. Additionally, 3D structures, manufactured from hybrids, can be converted into glass-ceramic or crystalline materials by heat treatment. Such 3D ceramic structures due to their good mechanical, thermal, and chemical properties are one of the sought-after engineering materials. Most hybrid preceramic polymers are metal-organic compounds derived from silicon with additional backbone chains consisting of carbon (C), nitrogen, oxygen (O), boron or metal atoms, such as: Hf, Zr, Al, Ti, Ge, V, Ce, Mo, Sn, Fe, Co, Ni, Pd, Pt, Cu, Ag, Au, W, etc. [21]. The backbone is connected to the side groups, which are mainly organic. The most common side groups are alkyl, vinyl, aryl, epoxy, and any other organic group, which can be involved in the photopolymerization (Fig. 22.5) [22].

In addition to homogeneous hybrid materials, composites are also used to obtain functionally structured ceramics. Generally, composites involve liquid or semi-liquid systems dispersed with fine ceramic particles as a feedstock or metal-organic resins, either in the form of inks or pastes. Polymer and ceramic particle composites are based on metal or semi-metal oxides, carbides, borides, nitrides, glass grains dispersed in organic monomers, such as oxymethylene, olefins, propylene or ethylene, urethanes, amides, ethers, esters, and acrylates (Fig. 22.5) [24].

However, composites have many disadvantages compared to hybrid organometallic monomer resins: the resolution of structures made of composites is limited by the particle size and the tendency to scatter light. Also, it is difficult to obtain a mixture of substances that is stable over a long period of time. Meanwhile, structures after heat treatment tend to shrink disproportionately in some directions, becoming porous or acquiring defects. The following light-based methods are commonly used in additive manufacturing for such materials formation: stereolithography (SL)-digital light processing (DLP) and two-photon polymerization (TPP), along with inkjet-based inkjet printing (IJP) and extrusion-based direct ink writing (DIW) [24, 25]. Indeed, the most promising method for obtaining high resolution and functionality for the production of ceramics is laser two-photon polymerization of monolithic hybrid materials with pyrolysis [20].

2.1 Synthesis of Hybrid Materials and Composites

Laser two-photon polymerization technology has the benefit of being able to use a wide range of materials [26]. The requirements for materials suitable for two-photon polymerization are very minimal: they must be transparent to the laser wavelength and must possess the characteristics for multi-photon absorption, which induces photopolymerization [27, 28]. In order to apply pyrolysis to the structures thus produced and convert them into pure inorganic ceramics or crystals, the chemical chain of materials must contain parts that do not tend to decompose to gas at high temperatures. Such materials are composites with inorganic nano/micro-particles or hybrid metal-organic prepolymers that are discussed in the previous paragraph and schematically depicted in Fig. 22.5, while their potential transformations into pottery are indicated by pink arrows. The sol-gel synthesis method is the most suitable and best studied method for the production of hybrid materials [29].

In brief, the sol-gel process entails preparing a precursor mix (a sol or a solution), which transforms into a more solid-like substance upon evaporation of the solvent, dehydration, and chemical cross-linking of its solid, liquid, or dissolved components [30]. Sols or solutions can often be transformed into ceramics through gel-like intermediates at temperatures that are significantly lower than the ones employed in traditional processing [29]. This occurs because the precursors used

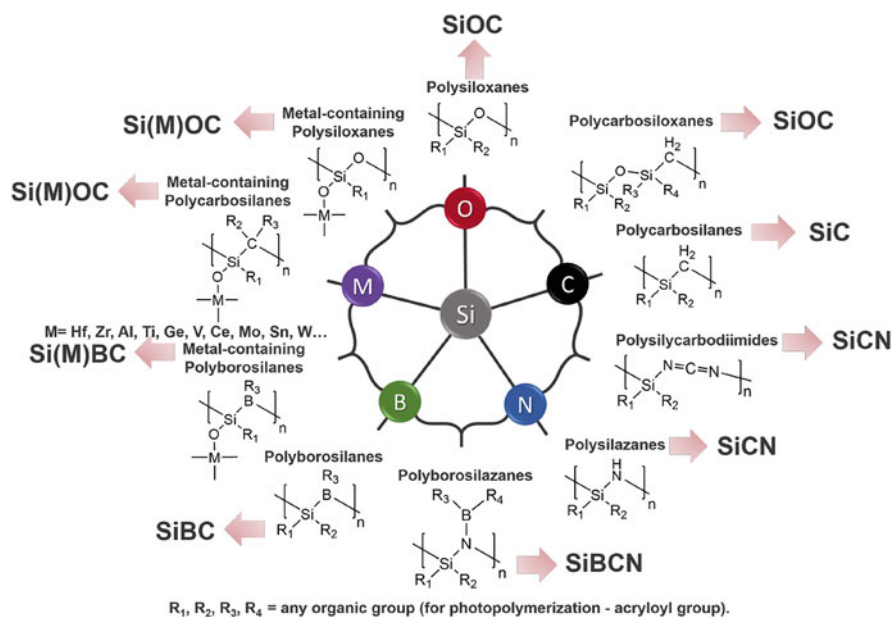


Fig. 22.5 Possible common types of silicon-based hybrid organometallic polymers in the Si-Me-O-C-N-B system used as precursors for ceramics. Reproduced from [23]

are intermixed at a molecular level and can react chemically to form a network of chemical bonds, a basis of ceramic materials.

To make it easier to understand the synthesis methodology, we present Fig. 22.6 as an example and discuss it below. The sol–gel process begins with the stabilization of an alkoxide of metal/semi-metal by organic molecules that are used as complexing ligands to provide chemical control over hydrolysis and condensation reactions, leading to form a stable suspension [31].

In the case of photocurable resins synthesis, organic acid having acryloyl group, for example, methacrylic acid, should be added to produce stable, photo-active, able to participate in photopolymerization precursors. Stabilization is carried out slowly by dropwise adding the organic acid to the alkoxide. After photopolymerization, hydrolysis is performed. During hydrolysis, water reacts nucleophilically with metal alkoxide to form hydroxide groups through the alkoxy groups contained in the metal alkoxide precursor. Acids or bases are used as catalysts for these reactions. The way the reaction occurs and its kinetic properties are principally influenced by the catalyst, the nature of the alkoxide group, and the employed solvent. Stabilized and hydrolyzed alkoxides of metals or semi-metals are added dropwise to each other. Typically, the alkoxide of the more active metal is added dropwise to the more passive one, thus forming a liquid solution–sol. The natural phenomenon that follows hydrolysis of alkoxide precursors is condensation (also called polycondensation or inorganic polymerization). In this process, hydroxyl groups react with each other to form oxo bridges ($-M-O-M-$) in combination with the simultaneous elimination of either a water or alcohol molecule [31–33]. In the presence of solvents and alcohol formed after hydrolysis, the condensation procedure is accelerated by heating ($\sim 90^\circ\text{C}$), depending on the solvents and alcohol formed after hydrolysis; as a result, the gels are sufficiently rigid and clear, so they can be polymerized with appropriate radiation [32]. Additionally, a photoinitiator may be added to the sol, depending on the employed light source.

2.2 Thermal Post-Processing Techniques for 3D Nanostructures

Commonly, hybrid organometallic 3D objects have similar mechanical properties to organic structures [34, 35]. However, hybrids have one major advantage—they can transform into pure inorganic amorphous, glassy, or crystalline structures [19, 20, 36]. As a result, the amplitude of the application of such structures increases significantly. Therefore, here we will describe the post-processing of 3D hybrid structures to obtain inorganic-amorphous or crystalline structures (see Fig. 22.7). We will use the well-known and widely used SZ2080TM [37] material to illustrate the processes.

The transformation of SZ2080TM from polymer to amorphous glass–ceramic was studied and described by Gailevičius et al. [19]. Subsequently, Merkininkaitė

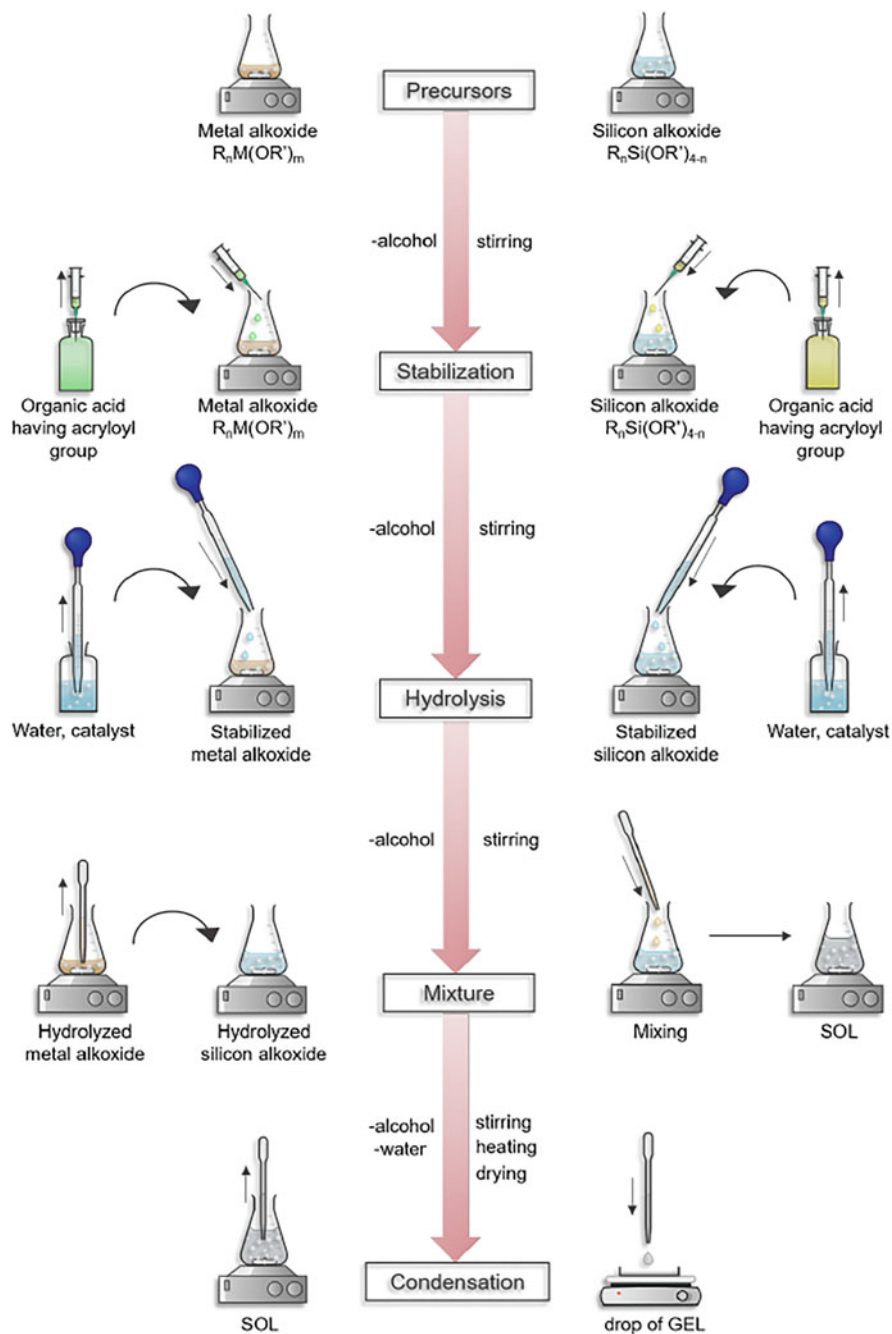


Fig. 22.6 Scheme of sol-gel synthesis of silicon-based organometallic prepolymer for laser photopolymerization. The scheme was prepared using free online chemix.org software

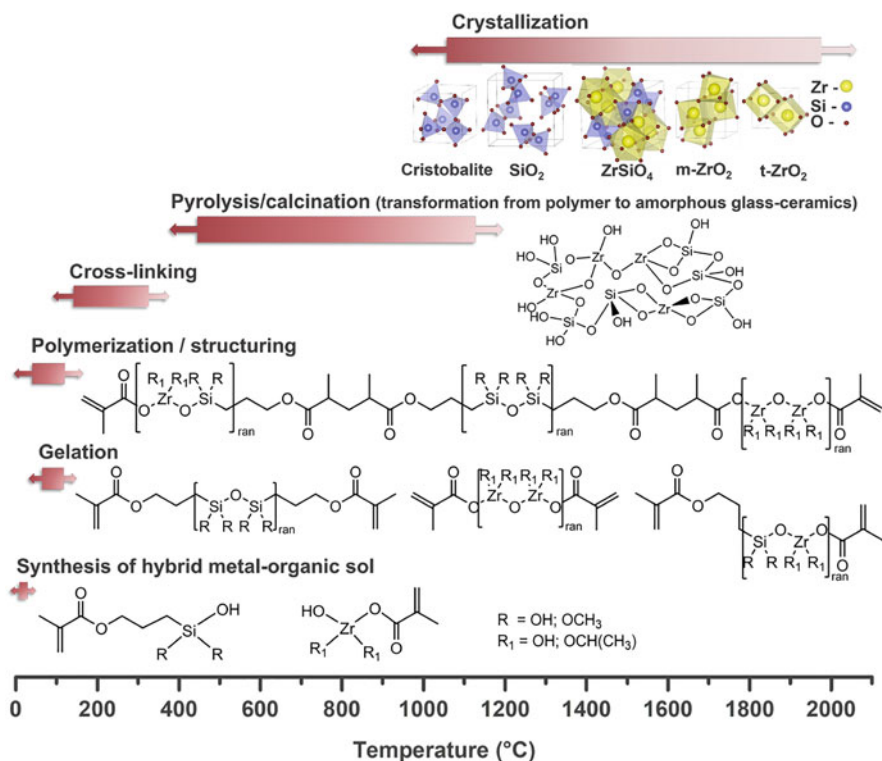


Fig. 22.7 Thermal transformation steps from synthesis to crystallization in Si–Zr organometallic system. Chemical structures and crystal lattices were reproduced from [19] and [20], respectively

et al. [20] investigated the dependence of crystallization on different variations in material composition and annealing temperature.

Fabrication of 3D inorganic derivatives commonly includes the following steps: First, synthesis of hybrid metal-organic prepolymer (sol- if metals alkoxides and/or siloxanes as precursors are used in the sol–gel method for the manufacture of the substance). Second, gelation, if necessary, depending on the precursors, is usually carried out at temperatures close to the boiling points of the solvents, and third photopolymerization is one of the methods that is visually explained in Fig. 22.4, or alternatively any other approach to obtain a 3D shape can be implemented. The early presented three steps are thoroughly described in the previous section.

Before the transformation of precursors into ceramic materials, a series of reactions, resulting in changes of composition and properties that are responsible for maintaining the shape after heat treatment, should be performed. Such a process is called cross-linking and can be initiated under different mechanisms [38]. Based on the chemical features of precursors, cross-linking occurs upon exposure to light or selective laser curing (the described case of photopolymerization), thermal effect (150 °C – 400 °C), electron-beam curing, chemical stimuli, and reactive plasma based on NH_3 , CH_4 , N_2 , H_2 , H_2O , O_2 , SiH_4 , BH_3 gases for cross-linking

at low temperatures ($<200\text{ }^{\circ}\text{C}$). Thermal cross-linking after photopolymerization is the most attractive and best studied for hybrid metal-organic materials. This technique induces hydrosilylation (Si-H/vinyl groups), transamination (evolution of amines, ammonia, or oligomeric silazanes), thermal polymerization (vinyl or allyl groups), and dehydrocoupling (Si-H/Si-H or Si-H/N-H groups) reactions causing the formation of organic/inorganic networks [22, 36] and slight structure densification.

The following high-temperature methods (usually at temperatures above $400\text{ }^{\circ}\text{C}$) for the organic–inorganic transformation of polymers into an amorphous glass, ceramics, or crystalline structures are pyrolysis, calcination, and crystallization. The parameters of structures after heating, such as structures of chemical composition, density, ceramic yield, shape, defects population, surface morphology, crystallinity are mainly influenced by the composition of the initial material, heating temperature, and its rate of rising and holding times, heating atmosphere, overpressure, or vacuum [39]. Such transformations involve the decomposition or rearrangement of chemical bonds, the formation of new chemical bonds, and the removal of the organic part from the matter. Usually, weight loss can reach $\approx 30\%$ [40] of the initial weight, while linear shrinkage $\approx 40\%$ [19] (linear shrinkage). Most of the precursors (individually for each composition) become amorphous glass/ceramic up to $1100\text{ }^{\circ}\text{C}$, and crystallization begins at higher temperatures (typically from $1200\text{ }^{\circ}\text{C}$ or the onset of crystallization can begin even at $2000\text{ }^{\circ}\text{C}$). The atmosphere has the most influential effect on the composition of the resulting ceramics. In an oxidizing environment, organic material is removed in the form of CO and CO₂ gas, so it is essential to adjust the rate of temperature rise to avoid porosity developing on the surface of the structure. In this case, oxides of metals or semi-metals are most likely to form, as well as using the SZ2080TM (see Fig. 22.7) as a precursor. The formation of free carbon in the structure is promoted by heating in an inert atmosphere such as Ar or N. Additionally, added pressure has been proven to result in high free carbon content, since it hinders carbothermal reactions at high temperatures. Contrary, heating in a vacuum or reducing atmosphere (H₂ or NH₃) promotes carbothermal reactions, resulting in the release of free carbon [22].

In summary, the optimal conditions for polymer-to-ceramic conversion extensively depend not only on the original precursor composition, but also on the atmosphere, heating rate, temperature, and many other factors. This is opening for new directions and applications of laser-made micro-optics under harsh conditions such as high-intensity radiation, temperature, acidic environment, pressure variations, which include open space, astrophotonics, and remote sensing.

3 Trends and Technical Applications

Here we provide some most promising trends and directly benefiting fields of applications, where specifically sub-100-nm scales/definition and extreme conditions such as temperature, pressure, mechanical, optical and chemical environment are

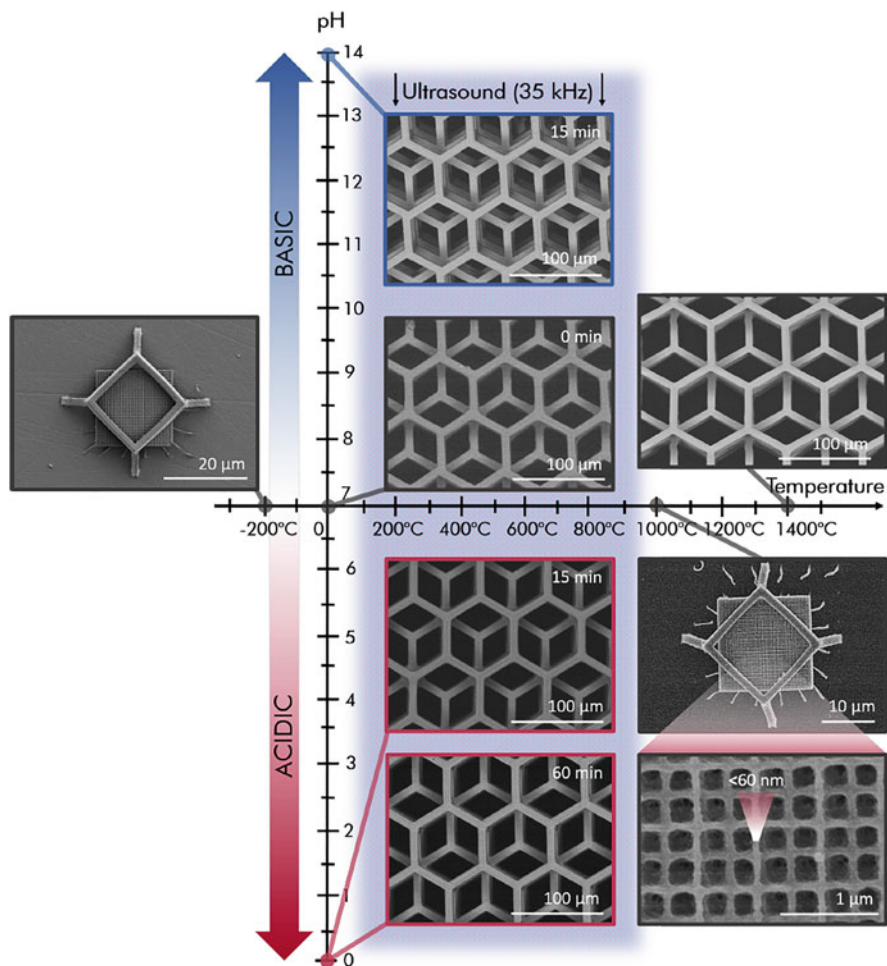


Fig. 22.8 Resistance of ceramic/crystalline 3D nano/micro-derivatives to aggressive chemicals, temperature, and ultrasound in Si/ZrO₂ system. Figure produced using results from [20]

playing critical roles. A graphically visualized map of 3D nanostructure resiliency is shown in Fig. 22.8, which confirms that ceramic micro–nano 3D structures withstand a wide range of temperatures (at least from -200°C to 1400°C), remain stable, and maintain sub-100-nm resolution throughout the pH range even under ultrasonic exposure. Technical applications are separated into these sub-topics: micro-optics, nanophotonics, micro-/nano-fluidics, micro-mechanics, and nano-electronics. We foresee that these fields will feature face the most benefit and list the current milestone achievements together with important details.

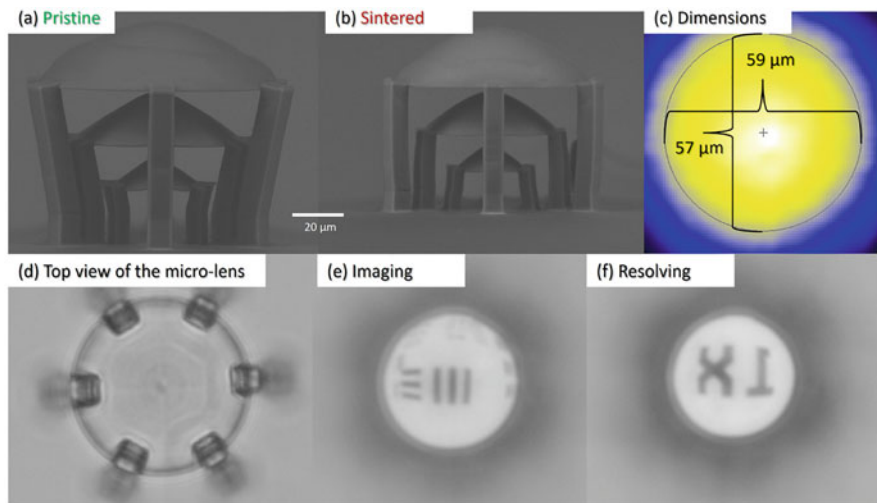


Fig. 22.9 An SEM image of compound micro-optical component stacked of 3 aspheric lenses: (a) pristine and (b) sintered. Geometrical characterization of the single lens diameter by optical profilometer (c), and its top view under OM (d). Validation of the same calcinated micro-lens imaging and resolving properties using 1951 USAF test target—imaged group 6 element 7 corresponds to the resolution of $4.39\ \mu\text{m}$ (228 lp/mm). As shown, the geometrical and material properties such as projected lens shape and optical transparency are preserved for quality functional performance. Figure adapted from [41], courtesy of Ms. D. G. Hernandez

3.1 Micro-Optics

For instance, a pilot study on laser 3D printing of inorganic free-form micro-optics was experimentally validated by the author group of this chapter. Ultra-fast laser nanolithography was employed for structuring hybrid organic–inorganic material SZ2080TM and followed by high-temperature calcination ($\sim 1000\ ^\circ\text{C}$) post-processing. The combination allowed the production of true 3D architectures and the heat treatment resulted in converting the material into a highly transparent inorganic substance. The produced miniature optical elements were characterized, and their optical performance was demonstrated (Fig. 22.9).

Finally, the concept was validated for manufacturing compound optical components such as stacked lenses [41]. This is extremely attractive for the implementation of LDW lithography-made glass optics in material processing, remote sensing, and astrophotonics. Within the limitation of the employed techniques and equipment in the referenced study, the refractive index n could not be precisely estimated, yet the preliminary measuring indicated an averaged value of ≈ 1.609 , which was reasonable and matched well with the $n = 1.617$ as previously reported for non-structured material in the literature [42]. The calcinated micro-lenses imaging and resolving properties were certified by 1951 USAF test target—imaged group 6

element 7 corresponding to a resolution of $4.39\ \mu\text{m}$ (228 lp/mm) that is matching with the reported data obtained with polymer micro-optics [43].

3.2 Nanophotonics

Additive manufacturing at small scales enables advances in 3D nanophotonic systems as a choice of high-refractive-index materials is limited especially. A recently developed process to fabricate complex 3D architectures out of fully dense titanium dioxide (TiO_2) with a $n = 2.3$ and nanosized critical dimensions required for sub-wavelength structures. The transmission electron microscopy analysis proved this material to be a rutile phase of nanocrystalline TiO_2 , with an average grain size of 110 nm and $<1\%$ porosity. Proof-of-concept woodpile 3D architectures with 300–600-nm beam dimensions exhibited a full photonic bandgap centered at 1.8–2.9 μm , as was revealed by Fourier-transform infrared spectroscopy and matching with plane wave expansion simulations [44]. The whole route protocol and resulting structures are shown in Fig. 22.10.

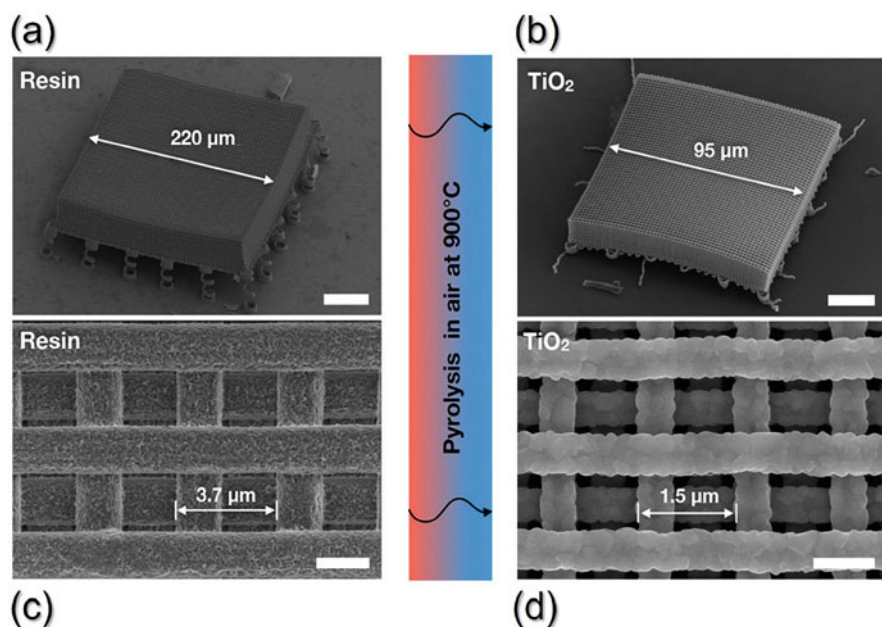


Fig. 22.10 Schematic representation of laser additive manufacturing of TiO_2 3D nanoarchitectures by SEM images. (a) Woodpile architectures were supported by a set of springs that decouple them from the substrate. (b) Titania woodpile structure was formed by calcination of the preceramic part. Representative TiO_2 magnified view before (c) and after (d) calcination at 750–900 °C. Scale bars are: (a) $50\ \mu\text{m}$, (b) $20\ \mu\text{m}$, (c) and (d) $2\ \mu\text{m}$, H – $1\ \mu\text{m}$ [44]. Reproduced with permission from the American Chemical Society. Copyright ©2020 by ACS

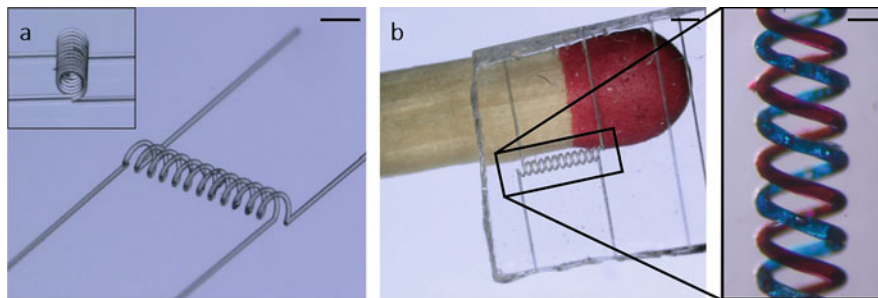


Fig. 22.11 Glass templates produced by LDW and thermal treatment: **(a)** Intertwined spirals (scale: $900\ \mu\text{m}$). **(b)** Resulting intertwined micro-fluidic spiral channels in fused-silica glass with a channel width of $74\ \mu\text{m}$. The channels were filled with dyes (see inset, scale: $140\ \mu\text{m}$). As can be seen, the 3D structures can be replicated with high fidelity and no deformations [45]. Reprinted with permission from Nature Communications. Copyright ©2019 by Nature Communications

3.3 *Micro-Fluidics*

Micro-fluidics is another field that is greatly benefiting from the true 3D shaping of glass structures. The topic, its challenges, and achievements are described in more detail by K. Sugioka in Chap. 30 of this book. Here we want to exemplify the fabrication of arbitrary three-dimensional suspended hollow microstructures in transparent fused-silica glass as a result of bench-marking current state of the art [45]. A micro-fluidic 3D intertwined mixer is shown in Fig. 22.11. The reported results were achieved by mixing SiO_2 nanopowder in the organic binder resin instead of sol-gel chemistry-derived hybrid photopolymer.

3.4 *Micro-Mechanics*

Ultrafast LDW multi-photon lithography opened a new dimension for the mechanical material engineering based on nano-architected additive manufacturing [47]. High-porosity (low mass density) objects with optimized internal 3D geometries in combination with thermal treatment enable the production of ductile, ultrastrong polymer-derived nanoceramics [46]. As an example, mechanical performance in SiOC nanolattices is shown in Fig. 22.12. SiOC is reported as the strongest, stiffest, and most resilient two-photon polymerizable material with pillars up to $20\ \mu\text{m}$ in diameter displayed plastic deformation and strength $>7\ \text{GPa}$. The developed 200-nm feature sizes were printed, with only 30% shrinkage upon pyrolysis.

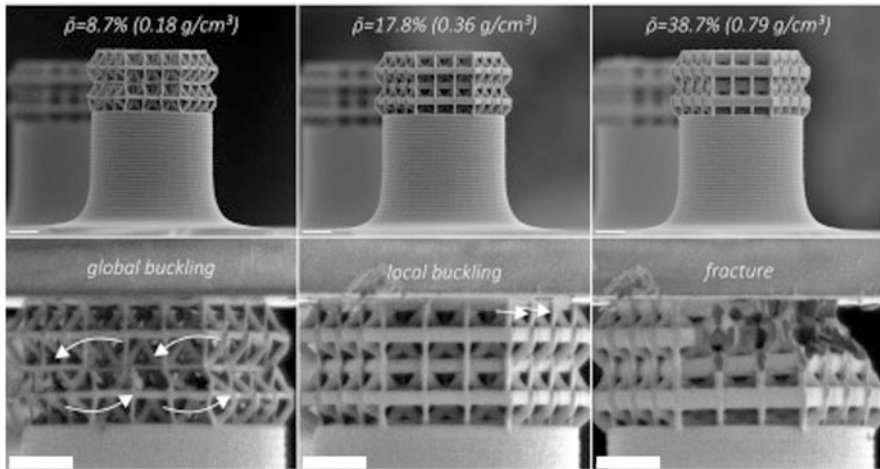


Fig. 22.12 Mechanical characterization of SiOC nanolattices: 3D structures before mechanical characterization (top) and at the moment of failure (bottom). Scale bars are all 5 μm . [46] Reprinted with permission from Elsevier. Copyright ©2019 by Elsevier

3.5 Nano-Electronics

For true 3D micro-/nano-electronic applications, conductive microstructures containing gold can be fabricated by simultaneous photopolymerization and photo-reduction LDW and pyrolysis. E. Blasco et al. have reported employing a photoresist consisting of water-soluble polymers and a gold precursor. The fabricated microstructures showed good conductivity and were successfully deployed for 3D connections between gold pads [48]. Though the ultrafast laser 3D lithography in combination with calcination is a relatively young and rapidly emerging field, that is studied in its feasibility sense, yet at the same time, it already produces some functional prototypes, such as ZnO-based UV photodetection with a large current on/off ration and high cycling stability [30]. This is of crucial importance for next-generation MEMS/NEMS and energy storage devices.

3.6 Sub-100-nm Challenges: Comparison of Current Achievements

In Fig. 22.13, essential publications in the LDW 3D lithography of inorganics are marked and dated accordingly. As an important criterion, the reports are ranked in resolution (feature dimension), specifically thresholding on sub-100-nm scale. Another plot represents the growing number of citations that shows increasing interest in the field. It is noted that during recent years the amount of original

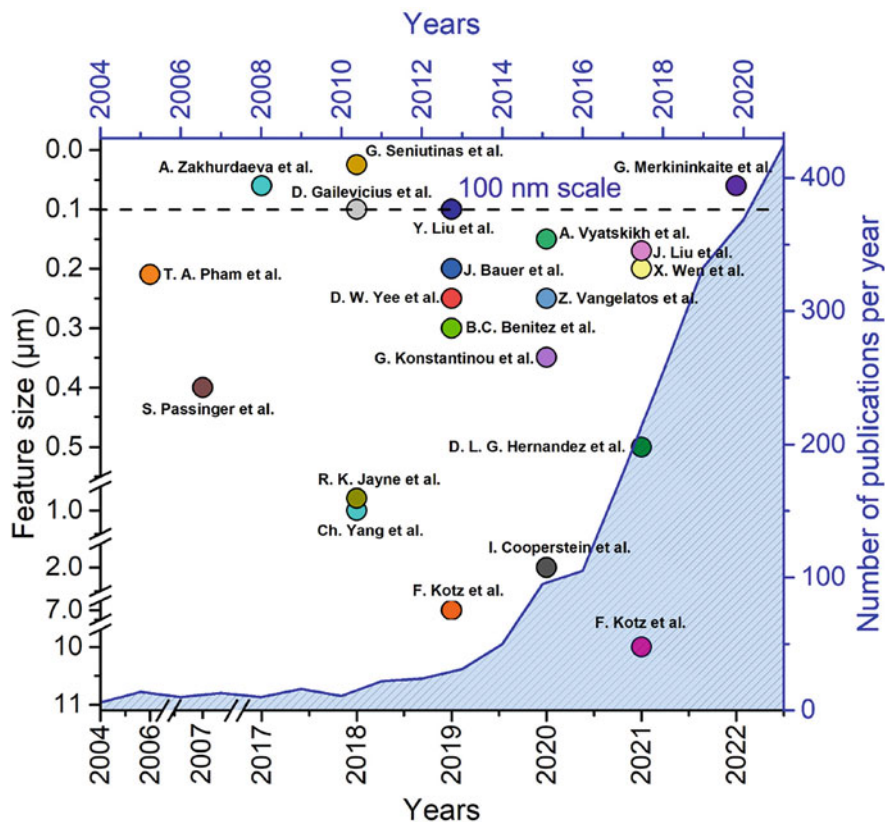


Fig. 22.13 Current achievements of 3D inorganic structure resolution in 3D lithography (corresponds to the black coordinate axis) and the number of publications per year (corresponds to the blue coordinate axis). The number of publications resulting from a search with keywords “3D, ceramic, printing” on scopus.com website, from 2004 to the December 2021 [18–20, 30, 41, 44–46, 49–61]

publications increases, and the density of the achievements concentrates toward the 100-nm benchmark, with sub-100 nm being repeatedly reached.

Sub-100-nm features can be fabricated using the stimulated emission depletion (STED) technique, which requires a more sophisticated two-wavelength laser setup and materials rather prepared suitable for that specific lithography purpose [62, 63], yet not for their functionality. Additionally, reaching dimensions below 60 nm is still not trivial task as shown in Fig. 22.14d), though it dramatically helps improving resolution to nearly 100 nm [63, 64]. While plasma etching helps fining the features (g) and pyrolysis/calcination offers downscaling (i–j), the later one is also converting the material into inorganic substances, which is way more useful for many technical applications. And as seen in (j), the achieved fine features are off-comparable dimensions to STED-made, yet without specific material optimization

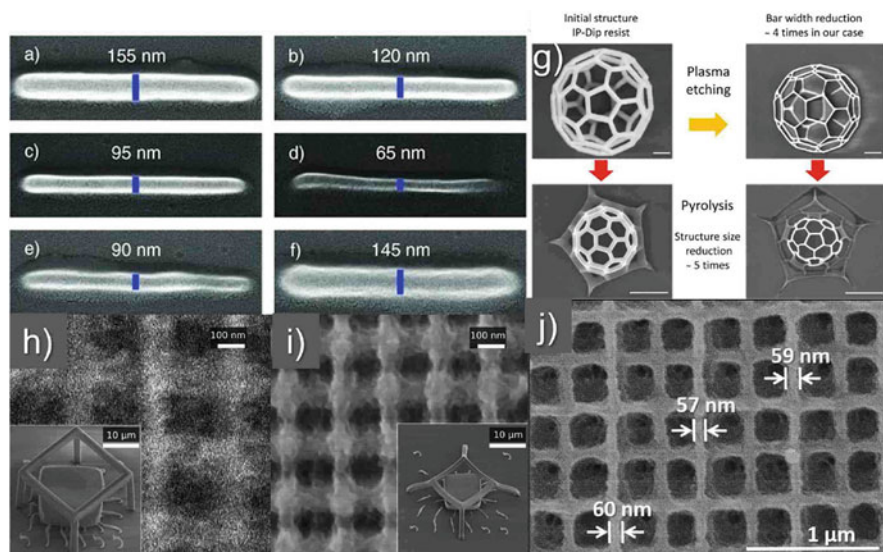


Fig. 22.14 Current achievements of sub-100-nm features via STED lithography (a–f), plasma and pyrolysis-assisted post-processing solutions (g), and (h–j), and inorganic structures obtained via calcination approach. Note that STED technique allowed achieving of 65-nm features of organic materials as shown in (d), yet further variations of depletion power resulted in enlargement of the primitive structures (e–f). In (h), a lattice structure out of SZ2080™ before and (i) after calcination is shown, with line widths reaching below 100 nm already in inorganic glass–ceramic material, whereas with the material tuned for inorganic substance, outcome results in reproducibly reached 60-nm homogeneous lines in a well-ordered lattice geometry, shown in (j). Scale bars represent 1 μm in (g). [18–20, 62]

and upgrading of setup to a multi-color exposure are not required. Finally, the calcination route ensures complete material conversion to inorganics, thus avoiding the variation of polymer degree of conversion that depends on exposure dose [65] and removes the photoinitiator in case it was used in the photoresin [41].

Currently, pure organic plant-derived resins compared to commercially available petroleum-based resins are offering competitive performance in material photosensitivity, mechanical properties, achievable 100-nm feature sizes [66], and even can offer naturally inherent bactericidal properties [67]. ~ 100 -nm suspended rods were made from vegetable oils thiol-ene/thiol-epoxy resins developed for the LDW 3D lithography as shown in Fig. 22.15a. We foresee that such resins can be explored for calcination purposes too, thus potentially enabling sub-100-nm features while involving only sustainable material processing.

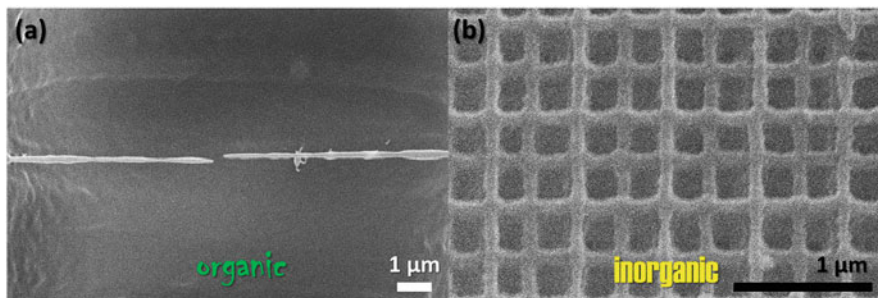


Fig. 22.15 \sim 100-nm suspended rods fabricated out of organic materials and \sim 65-nm line width reproducible inorganic template derived out of Si9:Zr1, (a) and (b), respectively [20, 66]. Both examples show that the LDW 3D multi-photon lithography (MPL) technique is readily available for sub-100-nm 3D fabrication out of diverse materials ranging from pure organic to completely inorganic via photopolymerization route

3.7 Emerging Applications

Table 22.0 summarizes the current achievements where LDW 3D lithography was used in combination with thermal post-treatment: reference, year, materials used, details of processing protocol, achieved dimensions, and targeted applications. As it is seen, various femtosecond laser setups of different wavelengths and pulse durations as well as repetition rates were applied, without a clear discrimination of 515-nm vs. 780–800-nm wavelengths and 100 fs vs. 300 fs pulse durations as well as 200 kHz or 80 MHz. Thus it can be deduced that the initial dimensions of the 3D structure, specific material, and optimized calcination protocol are determining the final dimensions of the produced feature. It should be noted that not all the groups were aiming for the highest resolution, rather for the specific application. On the other hand, supporting techniques such as helium-assisted microcasting can be used for employing hollow polymer templates for filling it with glass slurry and sequentially removing the template completely [100]. This results into fused-silica structures where the laser 3D structured polymer serves just as a sacrificial structure. Thus it is fascinating to see the approaches developed in ceramic industry are being re-implemented for micro- and nano-scales.

Figure 22.16 depicts of expected emerging laser and calcination made 3D nanostructured ceramic properties related to inherent material chemical compositions. Namely, thermal conductivity, chemical reactivity (inertness), optical, mechanical, and electromagnetic characteristics can have pronounced discrete values demanded by specific applications. The developments described in this chapter are compatible with the technology's capability of making multi-material polymer 3D structures [101], thus empowering to make multi-material inorganic–organic or inorganic–inorganic structures [49].

Finally, the eco-innovative aspect based on plant-derived optically 3D printable resins allows merging bio-renewable resources with the discussed calcination

Table 22.0 Current achievements of 3D inorganic structure resolution in 3D lithography

Nr.	Ref. year	Final material	Post-processing	Laser parameters and setup	Feat. size, nm	Applications
1.	[20] 2022	SiO ₂ , ZrSiO ₄ , t-ZrO ₂ , m-ZrO ₂	Heating, air, 1 h at 1000 °C, heating rate 5 °C/min.	Direct laser writing, $\tau = 300$ fs, $\lambda = 515$ nm, $f = 200$ kHz, $P_{\text{avg}} = 64$ μ W, 100x 1.4 NA objective, $v = 200$ μ m/s, $h = 0.1$ μ m (in both, x and y axes)	60	3D ceramic nanostructures that are resistant to extreme low and high temperatures and aggressive chemicals
2.	[30] 2021	Metal oxide semiconduc- tors (e.g., ZnO and Co ₃ O ₄)	Heating, O ₂ , 550 °C for 30 min, heating rate 20 °C/s	Homemade TPP system. A Ti: sapphire fs laser, $\lambda = 780$ nm, $\tau = 100$ fs, $f = 80$ MHz, 40x 1.3 NA objective, $P_{\text{avg}} = 7 - 20$ mW, $v = 0.5 - 5$ mm/s.	170	Optoelectronic and semiconductor devices
3.	[41] 2021	SiO ₂ , ZrO ₂	Heating, air, raising the temperature for 12 h until reaching 1100 °C and maintaining it for 3 h	$\lambda = 515$ nm of a Yb:KGW laser Pharos (Light Conversion Ltd.), $\tau = 300$ fs, $f = 200$ kHz, 63x 1.4 NA objective.	500	Micro-optics that are resistant to: high-intensity radiation, temperature, acidic environment, pressure variations
4.	[61] 2021	SiO ₂ doped with Er ³⁺ , Eu ³⁺ , Tm ³⁺ , Nd ³⁺ , and Yb ³⁺	Heating, nitrogen, 1300 °C for 240 min, heating rate 1 °C/s	Commercial 2PP AM system Nanoscribe Photonic Professional GT, 63x 1.4 NA or 25x 0.8 NA objectives, $\lambda = 780$ nm, $\tau = 100$ fs, $P_{\text{avg}} = 15 - 20$ mW, $v = 4 - 5$ mm/s	200	Optical applications: active photonics, non-Hermitian photonics, and quantum devices

5.	[60] 2021	Fused silica	Heating, samples sintered in vacuum at a pressure of 5×10^{-2} mbar, 2 h at 1300 °C. The heating and cooling rate was 3 K/min	Commercial lithography system Photonic Professional GT2 (Nanoscribe GmbH, Germany), 10×0.3 NA objective (from Nanoscribe GmbH, Germany), $\lambda = 780$ nm, slicing $5 \mu\text{m}$, $h=1 \mu\text{m}$, $v = 100$ mm/s, and laser power 80%	10,000	High-resolution glass components including optics, photonics, functional and engineered surfaces as well as lab-on-a-chip, life sciences, and biomedical engineering
6.	[56] 2020	Zr-DMAEMA	Laser extreme pyrolysis, Lighthouse Sprout-C 4 W, $\lambda = 532$ nm, $P_{\text{avg}} = 5\text{--}10$ mW	FemtoFiber pro NIR laser, $\lambda = 780$ nm, $\tau = 100$ fs, $f = 80$ MHz, 100×1.4 NA objective	250	Tailored scaffolds for artificial tissue and 3D patterning of local hierarchical nanostructures for 3D complex biomimetic materials and structures
7.	[52] 2020	SiOC	Heating, argon, the temperature was increased to 200 °C with a hold time of 2 h and 1000 °C for 1 h, 5 °C/min	Nanoscribe Professional GT. The laser source is an ultrafast Er-doped fiber laser system from Topica Photonics AG, $\lambda = 780$ nm, $\tau = 100$ fs, $f = 80$ MHz, 63×1.4 NA objective, $P_{\text{avg}} = 15$ mW, $v = 6 \mu\text{m/s}$	349	Ceramic-based micro-nozzle for micro-droplets delivery or micro-manipulation that can be realized and provide high robustness and chemical resistance
8.	[44] 2020	Rutile TiO ₂	Heating, air, 750–900 °C for 1 h, 3 °C/min	A commercially available two-photon lithography system-Photonic Professional GT, Nanoscribe GmbH. $P_{\text{avg}} = 12.5\text{--}20$ mW and $t_{\text{ex}} = 0.5 \times 10$ ms	150	Fabrication of components for micro-optics or 3D MEMS

(continued)

Table 22.2 (continued)

Nr.	Ref. year	Final material	Post-processing	Laser parameters and setup	Feat. size, nm	Applications
9.	[49] 2020	YAG, Nd:YAG	Heating, air, 200 °C for 2 h, 520 °C for 2 h, 620 °C for 2 h for amorphous inorganic, further 920–1500 °C 5 h for polycrystalline, 0.6 °C/min	Photonic Professional GT printer (Nanoscribe GmbH, Germany). 25x objective	2000	Optical components in high-intensity laser systems, which require heat resistance, or light sources in optical circuits
10.	[58] 2019	IP-Dip	Heating, argon, 450 °C for 12, 17 or 2 min, 10 °C/min	Photonic Professional GT, $\lambda = 780$ nm, 63x 1.4 NA objective, $P_{\text{avg}} = 16 - 27$ mW, $v = 15$ mm/s	100	Integrated optical components, 3D photonic integrated circuitry, anti-counterfeiting security labels, dye-free structural color printing
11.	[57] Nano-engi- neering 2019	SU-8	Heating, nitrogen, 300 °C 1 h, 900 °C 1 h, 5 °C/min	Coherent Mira 900D, $\lambda = 800$ nm, $\tau = 150$ fs, $f = 76$ MHz, 100 x 1.4 NA objective	300	Carbon nanowires: label-free impedance-based nanobiosensors, nanoparticle-based gas sensors, and electrochemical immunosensors
12.	[45] 2019	IP-S template, fused silica	Heating, air, 600 °C, 0.5 °C/min thermal debinding, 1300 °C, 3 °C/min sintering	Photonic Professional GT, 0.8 NA objective	7000	Micro-fluidics, flow-through synthesis, photonics or waveguiding applications in optics, and photonics

13.	[46] 2019	SiOC	Heating, vacuum, 1000 °C for 1 h. Heating at 1 °C/min. Cooling at 3 °C/min	Photonic Professional GT, FemtoFiber pro NIR laser, $\lambda = 780$ nm, $\tau = 100$ fs, $f = 80$ MHz, 63×1.4 NA objective, $v = 10$ $\mu\text{m/s}$, $P_{\text{avg}} = 16\text{--}36$ mW for octet lattices (with 200-nm lines)	200	Engineering applications, ranging from automotive to aerospace and energy systems
14.	[51] 2019	Metal oxide (ex. ZnO)	Heating, air, 500 °C, heating at 0.5 °C/min, cooling at 2 °C/min	Photonic Professional GT, 63×1.4 NA objective	250	Nanoelectromechanical system (NEMS), desulfurization agent, UV photodetector
15.	[19] 2018	Glass-ceramic, cristobalite SiO ₂ and tetragonal ZrO ₂	Heating, air, 1000–1500 °C	$\tau = 300$ fs, $\lambda = 515$ nm, $f = 200$ kHz objectives from 0.8 to 1.4 NA	100	Chemically resilient and high-temperature optical elements for sensors
16.	[55] 2018	IP-Dip, PEG-DA, PETA	–	Nanoscribe Photonic Professional GT, $\lambda = 780$ nm, 63×1.4 NA objective	950	Microstructures for IR imaging or deformable microscaffolds for living cell studies

(continued)

Table 22.2 (continued)

Nr.	Ref. year	Final material	Post-processing	Laser parameters and setup	Feat. size, nm	Applications
17.	[18] 2018	IP-Dip, SZ2080	Heating, nitrogen flow 100 sccm, 250 °C 1 h, 350 °C 1 h, 690 °C 1 h, Heating rate 5 °C/min. Plasma etching	Photonic Professional GT, Femtolasers fusion, $\lambda = 800$ nm, $f = 75$ MHz, $\tau = 20$ fs, 100x 1.4 NA objective	25	Micro-optical elements and 3D templates or microscaffolds for cell studies
18.	[50] 2018	Glassy carbon	Pyrolysis by rapid thermal processing	Nanoscribe direct write laser lithography system	1000	Carbon microelectrodes
19.	[53] 2017	Glassy carbon	Heating, vacuum, 900 °C	Nanoscribe 2PP setup, $P_{\text{avg}} = 30\text{--}33.6$ mW, $v = 25$ mm/s	60	Carbon-microelectromechanical systems (Carbon-MEMS) and nanoelectromechanical systems (Carbon-NEMS)
20.	[54] 2007	Anatase, rutile TiO ₂	Heating, 450 °C anatase, 650 °C rutile	Spectra Physics Tsunami, $\lambda = 780$ nm, $\tau = 120$ fs, $f = 80$ MHz, 100x 1.35 NA objective	400	3D inorganic photonic crystals
21.	[59] 2006	SiCN	Heating, nitrogen, 600 °C for 2 h, temperature rate 2 °C/min	Ti:sapphire laser, $\lambda = 780$ nm, $\tau = 100$ fs, $f = 80$ MHz, 1.4 NA objective, $P_{\text{avg}} = 100$ mW, $t_{\text{ex}} = 1$ ms	210	3D ceramic structures such as: tribological MEMS and chemical-resistant micro-fluidics

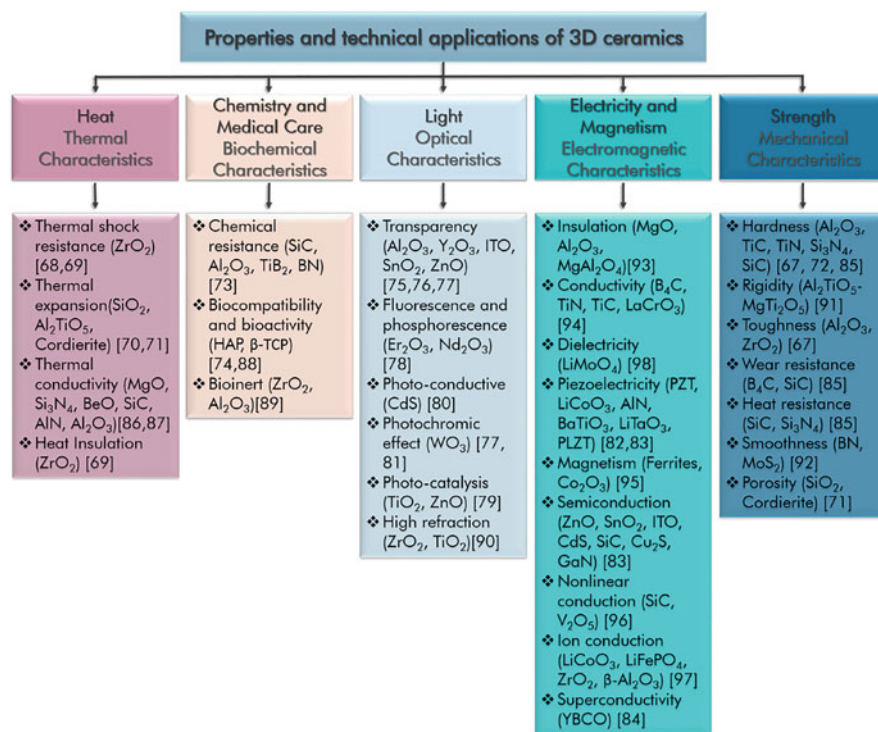


Fig. 22.16 Properties of 3D ceramics and their immediate possible and future potential technical applications [68–99]

method—as the organic matter is only used for templating and is evaporated eventually, thus it can allow selection of bio-based resins (such as derived from vegetable oils for instance) instead of petroleum ones [66]. As an example, an AESO (acrylated epoxidized soy oil)-based resin containing a natural diluent ethyl lactate can inherit up to 89% of the renewable carbon and offer multi-scale and multi-platform optical 3D structurability ranging from sub-micron to super-millimeter dimensions [102].

4 Summary and Conclusions

Here we have summarized recent advances and state of the art on ultrafast LDW lithography and its employment for additive manufacturing of 3D inorganic nanostructures. A specific focus was provided for material diversity, application impact, and sub-100-nm fabrication challenges. We included the combinations of precision optical 3D printing of hybrid organic–inorganic/composite materials

followed by high-temperature thermal post-treatment, which empowers fabrication of complex architectures and true glass, ceramic, and even crystalline structures. The synergistic developments in laser technology and material sciences are already leading to immediate applications in micro-optics, nano-fluidics, micro-mechanics, and nano-electronic fields. Together it joins the flexibility of 3D micro-/nano-prototyping with high performance, heavy-duty cycle, and high-resilience integrated devices.

In brief, a conclusion can be made that the LDW 3D nanolithography is no longer limited to (photo-)polymer materials as in combination with calcination technique it allows additive manufacturing of a wide variety of organics materials (including renewable plant-derived resins) that can be converted into diverse and functional inorganics. The possibility of the technology to make multi-material polymer-based 3D structures is also valid for making multi-material 3D inorganics. We emphasize that besides material conversion from hybrid to inorganic, the approach established a reliable route for downscaling the structures. This is of great interest as the LDW 3D MPL alone is struggling to reach below 100-nm features in a routine manner. Yet with the 40–60% feature reduction without the loss of geometry, it makes it viable for technology to produce complex shaped geometries and highest optically true 3D printable resolution. Additionally, the material densification while sintering is offering benefits of surface self-smoothing, which is important for micro-optics, nanophotonics, and fluidic applications. And finally, this is an indirect way to avoid the photoinitiators, which may be used during the exposure stage, but are removed while calcination. It makes a significant in material-structure optimization for delicate functions, such as artificially engineered refractive index by metamaterial geometries [103], and at the same time heavy-duty technical practical applications [104] such as ultra-compact wide-angle cameras based on multi-aperture free-form optical designs [105]. From the advances in 3D additive manufacturing perspective, its active micro-optics and nanophotonics or highly integrated systems including both of them are foreseen to benefit the most in the nearest future.

Acknowledgments We kindly acknowledge Dr. Maria Farsari (IESL-FORTH) and Prof. Saulius Juodkazis (SUT) for valuable information and fruitful discussions regarding materials and sintering processes. We are heartily thankful to PhD. students Edvinas Skliutas (VU) and Diana Laura Gonzalez Hernandez (at a time VU) for their help with SEM and contribution of some items presented in this chapter.

References

1. J. Stampfl, R. Liskas, A. Ovsianikov, *Multiphoton Lithography* (Wiley, London, 2016)
2. S. Maruo, O. Nakamura, S. Kawata, Three-dimensional microfabrication with two-photon-absorbed photopolymerization. *Opt. Lett.* **22**, 132–134 (1997)
3. K. Sugioka, Hybrid femtosecond laser three-dimensional micro-and nanoprocessing: a review. *Int. J. Extrem. Manuf.* **1**, 012003 (2019)

4. M. Mangirdas, A. Žukauskas, S. Hasegawa, Y. Hayasaki, V. Mizeikis, R. Buividas, S. Juodkazis, Ultrafast laser processing of materials: from science to industry. *Light Sci. Appl.* **5**, 16133 (2016)
5. L. Jonušauskas, D. Gailevičius, S. Rekštytė, T. Baldacchini, S. Juodkazis, M. Malinauskas, Mesoscale laser 3D printing. *Opt. Exp.* **27**(11), 15205–15221 (2019)
6. E. Skliutas, M. Lebedevaite, E. Kabouraki, T. Baldacchini, J. Ostrauskaite, M. Vamvakaki, M. Farsari, S. Juodkazis, M. Malinauskas, Polymerization mechanisms initiated by spatio-temporally confined light. *Nanophotonics* **10**(4), 1211–1242 (2021)
7. T. Baldacchini, *Three-Dimensional Microfabrication Using Two Photon Polymerization: Fundamentals, Technology, and Applications* (Elsevier, Amsterdam, 2015)
8. L. Yang, F. Mayer, U.H.F. Bunz, E. Blasco, M. Wegener, Multi-material multi-photon 3D laser micro- and nanoprinting. *Light Adv. Manuf.* **2**, 2021020003 (2021)
9. P. Kiefer, V. Hahn, M. Nardi, L. Yang, E. Blasco, C. Barner-Kowollik, M. Wegener, Sensitive photoresists for rapid multiphoton 3D laser micro- and nanoprinting. *Adv. Opt. Mater.* **8**, 2000895 (2020)
10. M. Malinauskas, A. Žukauskas, G. Bičkuskaitė, R. Gadonas, S. Juodkazis, Mechanisms of three-dimensional structuring of photo-polymers by tightly focussed femtosecond laser pulses. *Opt. Exp.* **18**(10), 10209–10221 (2010)
11. V. Hahn, T. Messer, N. Maximilian Bojanowski, E.R. Curticean, I. Wacker, R.R. Schroder, E. Blasco, M. Wegener, Two-step absorption instead of two-photon absorption in 3D nanoprinting. *Nat. Photon.* **15**, 932–938 (2021)
12. V. Hahn, P. Kiefer, T. Frenzel, J. Qu, E. Blasco, C. Barner-Kowollik, M. Wegener, Rapid assembly of small materials building blocks (voxels) into large functional 3D metamaterials. *Adv. Func. Mater.* **30**, 1907795 (2020)
13. M. Lago, A. Rodriguez, R. Sendón, J. Bustos, M. Nieto, P. Paseiro, Photoinitiators: a food safety review. *Food Addit. Contam. A: Chem. Anal. Control Exposure Risk Assess.* **32**, 779–798 (2015)
14. T. Bérces, *Chapter 3. The Decomposition of Aldehydes and Ketones*, volume 5 of *Comprehensive Chemical Kinetics* (Elsevier, Amsterdam, 1972)
15. E. Andrzejewska, *Three-Dimensional Microfabrication Using Two-photon Polymerization. Micro and Nano Technologies* (William Andrew Publishing, Oxford, 2016)
16. I. Bernardeschi, M. Ilyas, L. Beccai, A review on active 3D microstructures via direct laser lithography. *Adv. Intell. Syst.* **3**(9), 2100051 (2021)
17. J. Bauer, A.G. Izard, Y. Zhang, T. Baldacchini, L. Valdevit, Thermal post-curing as an efficient strategy to eliminate process parameter sensitivity in the mechanical properties of two-photon polymerized materials. *Opt. Exp.* **28**(14), 20362–20371 (2020)
18. G. Seniutinas, A. Weber, C. Padeste, I. Sakellari, M. Farsari, C. David, Beyond 100nm resolution in 3D laser lithography—post processing solutions. *Microelectron. Eng.* **191**, 25–31 (2018)
19. D. Gailevičius, V. Padolskytė, L. Mikoliānaitė, S. Šakirzanovas, S. Juodkazis, M. Malinauskas, Additive-manufacturing of 3D glass-ceramics down to nanoscale resolution. *Nanoscale Horizons* **4**, 647–651 (2019)
20. G. Merkininkaite, E. Aleksandravicius, M. Malinauskas, D. Gailevicius, S. Sakirzanovas, Laser additive manufacturing of Si/ZrO₂ tunable crystalline phase 3D nanostructures. *Opto-Electron. Adv.* **5**, 210077 (2022)
21. E. Balčiūnas, S.J. Baldock, N. Dreižė, M. Grubliauskaitė, S. Coultas, D.L. Rochester, M. Valius, J.G. Hardy, D. Baltrikienė, 3D printing hybrid organometallic polymer-based biomaterials via laser two-photon polymerization. *Polym. Int.* **68**(11), 1928–1940 (2019)
22. G. Barroso, Q. Li, R.K. Bordia, G. Motz, Polymeric and ceramic silicon-based coatings—a review. *J. Mater. Chem. A* **7**, 1936–1963 (2019)
23. R.K. Gupta, R. Mishra, S. Kumar, A. Ranjan, L. M. Manocha, N. Eswara Prasad, *Development of Polycarbosilane PCS Polymer and PCS-Derived SiC Fibers and Their Composites* (Springer, Berlin, 2020)
24. Z. Chen, Z. Li, J. Li, C. Liu, C. Lao, Y. Fu, C. Liu, Y. Li, P. Wang, Y. He, 3D printing of ceramics: a review. *J. Eur. Ceram. Soc.* **39**(4), 661–687 (2019)

25. P.A. Mathews, S. Koonisetty, S. Bhardwaj, P. Biswas, R. Johnson, P. Gadhe, Patent trends in additive manufacturing of ceramic materials (2020)
26. G. Merkininkaitė, D. Gailevičius, S. Šakirzanovas, L. Jonušauskas, Polymers for regenerative medicine structures made via multiphoton 3D lithography. *Int. J. Polym. Sci.* **2019**, 3403548 (2019)
27. M. Farsari, M. Vamvakaki, B. Chichkov, Multiphoton polymerization of hybrid materials. *J. Opt.* **12**, 124001 (2010)
28. M. Malinauskas, M. Farsari, A. Piskarskas, S. Juodkazis, Ultrafast-laser micro/nano-structuring of photo-polymers: a decade of advances. *Phys. Rep.* **533**, 1–31 (2013)
29. G.J. Owens, R.K. Singh, F. Foroutan, M. Alqaysi, C.M. Han, C. Mahapatra, H.W. Kim, J.C. Knowles, Sol-gel based materials for biomedical applications. *Progr. Mater. Sci.* **77**, 1–79 (2016)
30. J. Liu, Y. Liu, C. Deng, K. Yu, X. Fan, W. Zhang, Y. Tao, H.e Hu, L. Deng, W. Xiong, 3D printing nano-architected semiconductors based on versatile and customizable metal-bound composite photoresins. *Adv. Mat. Tech.* **7**(6) 2101230 (2022)
31. J. Livage, Sol-gel synthesis of hybrid materials. *Bull. Mater. Sci.* **22**, 201–205 (1999)
32. M. Oubaha, Introduction to hybrid sol-gel materials, in *World Scientific Reference of Hybrid Materials* (2019), pp. 1–36
33. B.L. Rivas, B.F. Urbano, J. Sánchez, Water-soluble and insoluble polymers, nanoparticles, nanocomposites and hybrids with ability to remove hazardous inorganic pollutants in water. *Front. Chem.* **6**, 320 (2018)
34. S. Fafenrot, N. Grimmelsmann, M. Wortmann, A. Ehrmann, Three-dimensional (3D) printing of polymer-metal hybrid materials by fused deposition modeling. *Materials* **10**(10), 1199 (2017)
35. E. Balčiūnas, S. Baldock, N. Dreize, M. Grubliauskaitė, S. Coultas, D. Rochester, M. Valius, J. Hardy, D. Baltruikiene, 3D printing hybrid organometallic polymer-based biomaterials via laser two-photon polymerisation. *Polym. Int.* **68**, 08 (2019)
36. Q. Wen, Z. Yu, R. Riedel, The fate and role of in situ formed carbon in polymer-derived ceramics. *Progr. Mater. Sci.* **109**, 100623 (2020)
37. A. Ovsianikov, J. Viertl, B. Chichkov, M. Oubaha, B. Macraith, I. Sakellari, A. Giakoumaki, D. Gray, M. Vamvakaki, M. Farsari, C. Fotakis, Ultra-low shrinkage hybrid photosensitive material for two-photon polymerization microfabrication. *ACS Nano* **2**, 2257–2262 (2008)
38. P. Colombo, G. Mera, R. Riedel, G.D. Sorarù, Polymer-derived ceramics: 40 years of research and innovation in advanced ceramics. *J. Am. Ceram. Soc.* **93**, 1805–1837 (2010)
39. P. Colombo, G. Mera, R. Riedel, Gian D. Sorarù, Polymer-derived ceramics: 40 years of research and innovation in advanced ceramics. *J. Am. Ceram. Soc.* **93**(7), 1805–1837 (2010)
40. L. Jonušauskas, D. Gailevičius, L. Mikoliunaite, D. Sakalauskas, S. Sakirzanovas, S. Juodkazis, Optically clear and resilient free-form μ -optics 3D-printed via ultrafast laser lithography. *Materials* **10**, 12 (2017)
41. D.L.G. Hernandez, S. Varapnickas, G. Merkininkaitė, A. Ciburyš, D. Gailevičius, S. Sakirzanovas, S. Juodkazis, M. Malinauskas, Laser 3D printing of inorganic free-form micro-optics. *Photonics* **8**(12), 577 (2021)
42. M. Nogami, Glass preparation of the ZrO₂-SiO₂ system by the sol-gel process from metal alkoxides. *J. Non-Crystall. Sol.* **69**, 415–423 (1985)
43. M. Schmid, F. Sterl, S. Thiele, A. Herkommer, H. Giessen, 3D printed hybrid refractive/diffractive achromat and apochromat for the visible wavelength range. *Opt. Lett.* **46**(10), 2485–2488 (2021)
44. A. Vyatskikh, R.C. Ng, B. Edwards, R.M. Briggs, J.R. Greer, Additive manufacturing of high-refractive-index, nanoarchitected titanium dioxide for 3D dielectric photonic crystals. *Nano Lett.* **20**(5), 3513–3520 (2020)
45. K. Arnold, S. Sevim, J. Puigmartí-Luis, A. Quick, M. Thiel, A. Hrynevich, P.D. Dalton, D. Helmer, B.E. Rapp, F. Kotz, P. Risch, Fabrication of arbitrary three-dimensional suspended hollow microstructures in transparent fused silica glass. *Nat. Commun.* **10**(1439) (2019)

46. J. Bauer, C. Crook, A.G. Izard, Z.C. Eckel, N. Ruvalcaba, T.A. Schaedler, L. Valdevit, Additive manufacturing of ductile, ultrastrong polymer-derived nanoceramics. *Matter* **1**(6), 1547–1556 (2019)
47. Z. Vangelatos, H.-M. Sheikh, P.-S. Marcus, C.-P. Grigoropoulos, V.-Z. Lopez, G. Flammourakis, M. Farsari, Strength through defects: A novel Bayesian approach for the optimization of architected materials. *Sci. Adv.* **7**, 2218 (2021)
48. E. Blasco, J. Muller, P. Muller, V. Trouillet, M. Schon, T. Scherer, C. Barner-Kowollik, M. Wegener, Fabrication of conductive 3D gold-containing microstructures via direct laser writing. *Adv. Mater.* **28**, 3592–3595 (2016)
49. C. Ido, I.S.R.K. Chaitanya, B. Alisa, L. Uriel, M. Shlomo, 3D printing of micrometer-sized transparent ceramics with on-demand optical-gain properties. *Adv. Mat.* **32**(28), 2001675 (2020)
50. Y. Cheng, C. Qun, P. Pumidech, L. Scott, G. Mallikarjunarao, L. Nickolay, V.B. Jill, 3D-printed carbon electrodes for neurotransmitter detection. *Angew. Chem. Int. Ed.* **57**(43), 14255–14259 (2018)
51. D.W. Yee, M.L. Lifson, B.W. Edwards, J.R. Greer, Additive manufacturing of 3D-architected multifunctional metal oxides. *Adv. Mater.* **31**(33), 1901345 (2019)
52. G. Konstantinou, E. Kakkava, L. Hagelüken, P. Vallachira W. Sasikumar, J. Wang, M.G. Makowska, G. Blugan, N. Nianias, F. Marone, H. Van Swygenhoven, J. Brugger, D. Psaltis, C. Moser, Additive micro-manufacturing of crack-free PDCs by two-photon polymerization of a single, low-shrinkage preceramic resin. *Addit. Manuf.* **35**, 101343 (2020)
53. A. Zakhurdaeva, P.I. Dietrich, H. Hölscher, Ch. Koos, J.G. Korvink, S. Sharma, Custom-designed glassy carbon tips for atomic force microscopy. *Micromachines* **8**(9), 285 (2017)
54. S. Passinger, M. Saifullah, C. Reinhardt, K.R.V. Subramanian, B. Chichkov, M. Welland, Direct 3D patterning of TiO₂ using femtosecond laser pulses. *Ad. Mat.* **19**, 1218–1221 (2007)
55. R.K. Jayne, Th. J. Stark, J.B. Reeves, D.J. Bishop, A.E. White, Dynamic actuation of soft 3D micro-mechanical structures using micro-electromechanical systems (MEMS). *Adv. Mater. Technol.* **3**(3), 1700293 (2018)
56. Z. Vangelatos, L. Wang, C.P. Grigoropoulos, Laser pyrolysis for controlled morphing and chemical modification on 3D microlattices. *J. Micromech. Microeng.* **30**, 055008 (2020)
57. B. Cardenas-Benitez, C. Eschebaum, D. Mager, J. Korvink, M. Madou, U. Lemmer, I. De Leon, S.O. Martinez-Chapa, Pyrolysis-induced shrinking of three-dimensional structures fabricated by two-photon polymerization: experiment and theoretical model. *Microsyst. Nanoeng.* **5**, 1–13 (2019)
58. Y. Liu, H. Wang, J. Ho, R. Ng, R. Ng, V. Hall-Chen, E. Koay, Z. Dong, H. Liu, C.W. Qiu, J. Greer, J. Yang, Structural color three-dimensional printing by shrinking photonic crystals. *Nat. Commun.* **10**, 1–8 (2019)
59. T.A. Pham, D.-P. Kim, T.-W. Lim, S.-H. Park, D.-Y. Yang, K.-S. Lee, Three-dimensional SiCN ceramic microstructures via nano-stereolithography of inorganic polymer photoresists. *Adv. Funct. Mater.* **16**(9), 1235–1241 (2006)
60. F. Kotz, A.S. Quick, P. Risch, T. Martin, T. Hoose, M. Thiel, D. Helmer, B.E. Rapp, Two-photon polymerization of nanocomposites for the fabrication of transparent fused silica glass microstructures. *Adv. Mat.* **33**(9), 2006341 (2021)
61. W. Wang, F. Ye, S. Yue, H. Guo, G. Gao, Y. Zhao, Q. Fang, C. Nguyen, X. Zhang, J. Bao, J.T. Robinson, P.M. Ajayan, J. Lou, X. Wen, B. Zhang, 3D-printed silica with nanoscale resolution. *Nat. Mater.* **20**, 1506–1511 (2021)
62. J. Fischer, G. von Freymann, M. Wegener, The materials challenge in diffraction-unlimited direct-laser-writing optical lithography. *Adv. Mater.* **22**, 3578–3582 (2010)
63. J. Fischer, M. Wegener, Three-dimensional optical laser lithography beyond the diffraction limit. *Laser Photon. Rev.* **7**, 22–44 (2013)
64. R. Wollhofen, J. Katzmann, C. Hrelescu, J. Jacak, T.A. Klar, 120 nm resolution and 55 nm structure size in STED-lithography. *Opt. Exp.* **21**, 10831–10840 (2013)
65. A. Zukauskas, I. Matulaitiene, D. Paipulas, G. Niaura, M. Malinauskas, R. Gadonas, Tuning the refractive index in 3D direct laser writing lithography: towards GRIN microoptics. *Laser. Photon. Rev.* **9**(6), 706–712 (2015)

66. S. Grauzeliene, A. Navaruckiene, E. Skliutas, M. Malinauskas, A. Serra, J. Ostrauskaite, Vegetable oil-based thiol-ene/thiol-epoxy resins for laser direct writing 3D micro-/nano-lithography. *Polymers* **13**, 872 (2021)
67. A. Navaruckiene, E. Skliutas, S. Kasetaitė, S. Rekštyte, V. Raudonienė, D. Bridziuvienė, M. Malinauskas, J. Ostrauskaite, Vanillin acrylate-based resins for optical 3D printing. *Polymers* **12**(2), 397 (2020)
68. P. Boch, J.-C Niece, *Ceramic Materials: Processes, Properties and Applications* (2010)
69. J. Binner, M. Porter, B. Baker, J. Zou, V. Venkatachalam, V.R. Diaz, A. D'Angio, P. Ramanujam, T. Zhang, T.S.R.C. Murthy, Selection, processing, properties and applications of ultra-high temperature ceramic matrix composites, UHTCMCs—a review. *Int. Mater. Rev.* **65**(7), 389–444 (2020)
70. R. Bermejo, L. Llanes, P. Supancic, T. Lube, Thermal shock behaviour of an $\text{Al}_2\text{O}_3/\text{ZrO}_2$ multilayered ceramic with residual stresses due to phase transformations. *Key Eng. Mater.* **290**, 191–198 (2005)
71. W. Liu, Y. Xie, Z. Deng, Y. Peng, J. Dong, Z. Zhu, D. Ma, Z. Yi, G. Zhang, X. Wang, Preparation of Al_2TiO_5 ceramic fibers and thermal expansion, insulation, and strength of ZrO_2 - Al_2TiO_5 fiberboards (2021)
72. Z.L. Belal M.S. Elmaghraby, A.I.M. Ismail, Thermal expansion, physico-mechanical properties and microstructure of cordierite synthesized from different starting materials. *Int. Ceram. Rev.* **64**, 209–213 (2015)
73. E. Bajraktarova Valjakova, V. Korunoska-Stevkovska, B. Kapusevska, N. Gigovski, C. Bajraktarova Misevska, A. Grozdanov, Contemporary dental ceramic materials, a review: Chemical composition, physical and mechanical properties, indications for use. *Open Access Macedonian J. Med. Sci.* **6**, 1742 (2018)
74. E. Moustafa, Hybridization effect of BN and Al_2O_3 nanoparticles on the physical, wear, and electrical properties of aluminum AA1060 nanocomposites. *Appl. Phys. A*, **127**, 1–9 (2021)
75. Q. Chen, B. Zou, Q. Lai, Y. Wang, R. Xue, H. Xing, X. Fu, C. Huang, P. Yao, A study on biosafety of HAP ceramic prepared by SLA-3D printing technology directly. *J. Mech. Behav. Biomed. Mater.* **98**, 327–335 (2019)
76. H.M. Oh, Y.J. Park, H.N. Kim, J.W. Ko, H.K. Lee, Effect of milling ball size on the densification and optical properties of transparent Y_2O_3 ceramics. *Ceram. Int.* **47**(4), 4681–4687 (2021)
77. A. Solodar, R. Drevinskas, P. Kazansky, I. Abdulhalim, A. Cerkauskaitė, Ultrafast laser induced nanostructured ITO for liquid crystal alignment and higher transparency electrodes. *Appl. Phys. Lett.* **113**, 081603 (2018)
78. T.D. Nguyen, L.P. Yeo, T.C. Kei, D. Mandler, S. Magdassi, A.I.Y. Tok, Efficient near infrared modulation with high visible transparency using SnO_2 - WO_3 nanostructure for advanced smart windows. *Adv. Opt. Mater.* **7**(8), 1801389 (2019)
79. L. Wang, B. Lu, X. Liu, Y. Shi, J. Li, Y. Liu, Fabrication and upconversion luminescence of novel transparent Er_2O_3 ceramics. *J. Eur. Ceram. Soc.* **40**(4), 1767–1772 (2020)
80. K. Hashimoto, H. Irie, A. Fujishima, TiO_2 photocatalysis: a historical overview and future prospects. *Jpn. J. Appl. Phys.* **44**(12), 8269–8285 (2005)
81. H. Yin, A. Akey, R. Jaramillo, Large and persistent photoconductivity due to hole-hole correlation in CdS . *Phys. Rev. Mater.* **2**, 084602 (2018)
82. Y. Yao, D. Sang, L. Zou, Q. Wang, C. Liu, A review on the properties and applications of WO_3 nanostructure based optical and electronic devices. *Nanomaterials* **11**(8), 2136 (2021)
83. S. Trolhier-McKinstry, S. Zhang, A.J. Bell, X. Tan, High-performance piezoelectric crystals, ceramics, and films. *Annu. Rev. Mater. Res.* **48**(1), 191–217 (2018)
84. B. Szafraniak, Ł. Fuśnik, J. Xu, F. Gao, A. Brudnik, A. Rydosz, Semiconducting metal oxides: SrTiO_3 , BaTiO_3 and BaSrTiO_3 in gas-sensing applications: a review. *Coatings* **11**(2) (2021)
85. D. Mendes, D. Sousa, An. C. Cerdeira, L. C.J. Pereira, A. Marques, J. Murta-Pina, A. Pronto, I. Ferreira, Low-cost and high-performance 3D printed YBCO superconductors. *Ceram. Int.* **47**(1), 381–387 (2021)

86. Z. Chen, Z. Li, J. Li, C. Liu, Ch. Lao, Y. Fu, C. Liu, Y. Li, P. Wang, Y. He, 3D printing of ceramics: a review. *J. Eur. Ceram. Soc.* **39**(4), 661–687 (2019)
87. K. Watari, High thermal conductivity non-oxide ceramics. *J. Ceram. Soc. Jpn.* **109**(1265), S7–S16 (2001)
88. S. Thapliyal, *Manufacturing and characterization of a 3D-printable, antibacterial, magnesium oxide nanoparticles reinforced ABS filament*. Ph.D. Thesis, 04 2017
89. B. Leukers, H. Güllkan, S. Irsen, S. Milz, C. Tille, H. Seitz, M. Schieker, Biocompatibility of ceramic scaffolds for bone replacement made by 3D printing. *Materialwiss. Werkstofftech.* **36**, 781–787, 12 (2005)
90. X. Du, S. Fu, Y. Zhu, 3D printing of ceramic-based scaffolds for bone tissue engineering: an overview. *J. Mater. Chem. B* **6**, 06 (2018)
91. K. Weber, D. Werdehausen, P. König, S. Thiele, M. Schmid, M. Decker, P.W. De Oliveira, A. Herkommer, H. Giessen, Tailored nanocomposites for 3D printed micro-optics. *Opt. Mater. Exp.* **10**(10), 2345–2355 (2020)
92. T. Shimazu, H. Maeda, E.H. Ishida, M. Miura, N. Isu, A. Ichikawa, K. Ota, High-damping and high-rigidity composites of Al_2TiO_5 – MgTi_2O_5 ceramics and acrylic resin. *J. Mater. Sci.* **44**, 93–101 (2009)
93. J. Wang, Extrusion-based 3D printing of macro/microstructures for advanced lithium/sodium batteries (2019)
94. Z. Liu, J. Yu, P. Li, W. Xiaolong, Z. Yusong, X. Chu, X. Wang, H. Li, Z. Wu, Band alignments of $-\text{Ga}_2\text{O}_3$ with MgO , Al_2O_3 and MgAl_2O_4 measured by X-ray photoelectron spectroscopy. *J. Phys. D Appl. Phys.* **52**, 295104 (2019)
95. C. Han, R. Babicheva, J. Dong Qiu Chua, U. Ramamurty, S. B. Tor, C. N. Sun, K. Zhou, Microstructure and mechanical properties of (TiB+TiC)/Ti composites fabricated in situ via selective laser melting of Ti and B_4C powders. *Addit. Manuf.* **36**, 101466 (2020)
96. K.A. Hamzah, C.K. Yeoh, M.M. Noor, P.L. Teh, Y.Y. Aw, S.A. Szazi, W.M.A.W. Ibrahim, Mechanical properties and thermal and electrical conductivity of 3D printed ABS-copper ferrite composites via 3D printing technique. *J. Thermoplast. Compos. Mater.* **35**(1), 3–16 (2022)
97. R. Venkatkarthick, J. Qin, A new 3D composite of V_2O_5 -based biodegradable ceramic material prepared by an environmentally friendly thermal method for supercapacitor applications. *Environ. Technol. Innovation* **22**, 101474 (2021)
98. Li B. Chen Z. Mi S.-Lao C. Liu C., Cheng X, Fabrication and characterization of 3D-printed highly-porous 3D LiFePO_4 electrodes by low temperature direct writing process. *Materials* **8**, 934 (2017)
99. M. Väättäjä, H. Kähäri, K. Ohenoja, M. Sobocinski, J. Juuti, H. Jantunen, 3D printed dielectric ceramic without a sintering stage. *Sci. Rep.* **8**, 10 (2018)
100. J. Kopfler, T. Frenzel, J. Schamlian, M. Wegener, Fused-silica 3D chiral metamaterials via helium-assisted microcasting supporting topologically protected twist edge resonances with high mechanical quality factors. *Adv. Mater.* **33**, 2103205 (2021)
101. S. Rekstyte, E. Kaziulionyte, E. Balciunas, D. Kaskelyte, M. Malinauskas, Direct laser fabrication of composite material 3D microstructured scaffolding. *J. Laser Micro. Nanoen.* **9**, 25–30 (2014)
102. E. Skliutas, M. Lebedevaite, S. Kasetaitė, S. Rekstyte, S. Lileikis, J. Ostrauskaite, M. Malinauskas, A bio-based resin for a multi-scale optical 3D printing. *Sci. Rep.* **10**, 9758 (2020)
103. T. Gissibl, S. Thiele, A. Herkommer, H. Giessen, Sub-micrometre accurate free-form optics by three-dimensional printing on single-mode fibres. *Nat. Commun.* **7**, 11763 (2016)
104. A. Butkute, L. Cekanavičius, G. Rimselis, D. Gailevicius, V. Mizeikis, A. Melninkaitis, T. Baldacchini, L. Jonusauskas, M. Malinauskas, Optical damage thresholds of microstructures made by laser three-dimensional nanolithography. *Opt. Lett.* **45**, 13–16 (2020)
105. A. Toulouse, J. Drozella, P. Motzfeld, N. Fahrbach, V. Aslani, S. Thiele, H. Giessen, A.M. Herkommer, Ultra-compact 3D-printed wide-angle cameras realized by multi-aperture freeform optical design. *Opt. Exp.* **30**, 707–720 (2022)